(1)

Experimental studies on the phase relations of manganese silicate minerals and their application to the natural occurrences

TAKAHASHI KOSEI

1994

CONTENTS

Experimental studies on the phase relations of manganese silicate minerals and their application to the natural occurrences

TAKAHASHI KOSEI

Abstract

Experimental studies on the phase relations of Si - rich braunite and manganese pyroxenoids have been carried out to analyse their natural occurrences. The Si - rich braunite with maximum 12.37 wt% SiO_2 component has been found at the Hikari mine in south west Hokkaido, Japan. The single crystal of braunite shows the zonal variation of SiO_2 content and the increase of divalent cation contents from the core to the edge. The Si - rich composition is represented by the formula $Mn^{3+}_{6-2x}(Mn^{2+}, Mg, Ca)_{1+x}\ Si_{1+x}O_{12}$ where x is up to 0.22. The formula represents the substitution of $2Mn^{3+} \leftrightarrow (\ Mn^{2+}, Mg, Ca\ ) + Si^{4+}$. The Mg substitution seems to be deeply correlated with Si substitution, while the Ca content is independent of Si substitution in Si - rich braunite.

Experimental study for confirming the solubility of "$MgSiO_3$" molecule in braunite has been carried out at 1100 ˚C in open air circamstances. The solubility limit was determined to be x = 0.2 of the formula $(Mn^{3+}_{6-2x}Mg_x\ Si_x)Mn^{2+}SiO_{12}$ from the change of the cell parameters. For x > 0.2 braunite coexists with tephroite which has a constant composition of $(Mn_{1.4}\ Mg_{0.6})\ SiO_4$.

Phase relations in the manganese rich portion of the system $MnSiO_3$-$MgSiO_3$-$CaSiO_3$ have been determined experimentally under the conditions of

700 °C - 1200 °C and 0 - 10 kb. The phases present were rhodonite, pyroxmangite, bustamite and kanoite. Each phase showed a limited solid solution and its stability field was changed depending on pressure and temperature. Phase assemblages, rhodonite-pyroxmangite, rhodonite-bustamite, pyroxmangite-kanoite, kanoite-bustamite and rhodonite-pyroxmangite-bustamite were found to be stable under the conditions. From these results, distribution coefficient K_D for respective coexisting phases were determined. The two - phase region of pyroxmangite-rhodonite shifts toward the Mn-rich and Mg-poor side in the Mn - Mg - Ca diagram with increasing pressure and/or decreasing temperature. The two phase region of pyroxmangite-rhodonite at 700°C-4kbar showed a good agreement with the compositional range of naturally coexisting pairs of pyroxmangite and rhodonite from the Tatehira mine, southwestern Hokkaido, Japan. The formation temperatures or pressures of coexisting two phases from other localities were also estimated using the experimentally determined K_D.

General Introduction

Manganese silicate minerals have been found at numerous localities, and they are typically contained in metamorphosed manganese - bearing rocks. Among them, the formation of pyroxenoids, $R^{2+}SiO_3$ (R = Mn, Mg, Ca, Fe) and tephroite $Mn^{2+}{}_2SiO_4$,tends to be relatively attributed to the high - grade metamorphism from the greenshist to the granulite facies. On the other hand, braunite $3Mn_2O_3 \cdot MnSiO_3$ is rather found in the low - grade metamorphic zone of manganese deposits. In both cases, the $MnSiO_3$ component plays an important role on the assemblages of manganese minerals. However, the phase relations have not been sufficiently studied because of the mixed valence nature of manganese ion and the resulting difficulty of the experiments.

The author has been analyzed natural specimens that include these mineral assemblages metamorphosed with different grades, and also carried out the experimental work to construct the phase diagrams of these manganese silicate minerals to be used for the estimation of the pressure, temperature conditions for the formations of natural mineral assemblages.

The coexistence of the pyroxenoids in metamorphosed manganese - bearing rocks has been described by many previous workers. Although the phase relations for the pure $MnSiO_3$ composition are reasonably well known, these results could not be used to determine the P - T conditions of natural pyroxenoids because the natural pyroxenoids have large and various cationic substitutions. In addition, since rhodonite structure has five cation sites, pyroxmangite, seven and bustamite, three, the various possibilities of cation distributions among them make it difficult to apply any mixing model to these systems. In this paper,

therefore, the author developed a geothermometer and geobarometer for these phases in the $MnSiO_3$-$MgSiO_3$-$CaSiO_3$ ternary system by using the experimentally determined K_D (distribution coefficient) with temperature, pressure and the third component.

Part 1 - Si-rich braunite

1 - 0 Introduction

Braunite, $3Mn_2O_3 \cdot MnSiO_3$ or $Mn^{3+}{}_6Mn^{2+}SiO_{12}$, has been found at numerous localities, and it is typically attributed to low-grade metamorphism of manganese rich sediments. The ideal formula of braunite requires 9.9 wt% SiO_2 component and most analyses of natural braunite fall in the range 1.00 ±0.03 Si in the formula (Abs-Wurmbach et al. 1983). But a few natural braunite has been reported with slightly higher silica content (maximum 11 wt%) and the excess is considered to be submicroscopic inclusions of quartz (Abs-Wurmbach et al. 1983, Momoi et al. 1982).

In the system Mn-Si-O, Muan (1959) estimated the existence of a wide range solid solution of braunite above 800 °C at various levels of oxygen partial pressure. But experimental studies by Abs-Wurmbach (1980, et al. 1983) and by Hino et al. (1977) indicated a very limited solubility of SiO_2 component in air and under hydrothermal conditions. Abs-Wurmbach (1980) also reported that the composition of braunite equilibrated with excess silica from 1000 °C to 1100 °C becomes Si / (Mn + Si) = 0.15, which corresponds to x = 0.235 of $Mn^{2+}{}_{1+x}Mn^{3+}{}_{6-2x}Si_{1+x}O_{12}$.

Braunite has a tetragonal cell and the structure consists of two kinds of sheets *A* and *B*,which are vertical to the *c* axis ; the *A* sheet ($2Mn_2O_3$) consists of Mn^{3+} ions in octahedral coordination and the *B* sheet ($MnSiO_3 \cdot Mn_2O_3$) consists of Mn^{2+} ions in cubic coordination, Mn^{3+} ions in

octahedral coordination and Si^{4+} ions in tetrahedral coordination. The stacking sequence of the sheet in unit cell is represented by $[AB]_4$. The bixbyite (Mn_2O_3)-braunite $3Mn_2O_3 \cdot MnSiO_3$ series which is deficient of silica content was explained by stacking variations of the above polyhedral layers (Moore and Araki, 1976).

Braunite II ($7Mn_2O_3 \cdot MnSiO_3$) (De Villers et al., 1967) also has a tetragonal cell and the structure consists of three kinds of sheets *A*, *A'* and *B*,which are vertical to the *c* axis ; the *A* and *B* sheet are samse as braunite and *A'* sheet ($2Mn_2O_3$) consists of Mn^{3+} ions in octahedral coordination. *A'* sheet structure is the distorted *A* sheet structure. The stacking sequence of the sheet in unit cell is represented by $[ABAA']_4$ (Moore and Araki, 1976). From this structure, braunite II contains less amount of SiO_2 content than braunite composition.

Another braunite group mineral is neltnerite ($3Mn_2O_3 \cdot CaSiO_3$) described by Baudracco et al., (1982) that substitute calcium for manganese ion in the divalent site.

The electron microscopic study of natural bixbyite-braunite series by de Villiers and Buseck (1989) revealed the presence of several sheet assemblages as expected. They showed that SiO_2 content of bixbyite-braunite series can vary from 0 to 10 wt% by changing the stacking sequence of *A* and *B* sheet. However, no stacking sequences were observed with respect to the excess of SiO_2 of braunite.

The present paper reports a new occurrence of Si - rich braunite and the results of experimental study on a limited part of the system $MnSiO_3$ - $MgSiO_3$ -

Mn_2O_3 which is relevant to the excess of SiO_2 component in braunite, and discuss about the mechamisum of the substitution comparing the compositions of Si - rich braunite with that of braunite II.

1 - 0 - 1 Natural Occurrences

Braunite from the Hikari mine in southwest Hokkaido, Japan contains an excess of silica content. The mine consists of Paleozoic manganese oxide deposits and spindle shape ore bodies are hosted in red chert and are folded complicatedly. Specimens were collected from the mining dumps. The ores consist of braunite, rhodochrosite and minor barite in order of decreasing modal abundance. Rhodochrosite veins include some idiomorphic braunite cut the massive braunite parts. The maximum size of idiomorphic braunite is 30 μm and the average size is 20 μm. These occurrences shows that this mine have secondary got a low grade hydrothermal alterations.

1 - 1 Compositional Variations

1 - 1 - 1 Si - rich braunite

Chemical composition was determined with a JEOL 733 electron microprobe in Hokkaido university. The operating parameters were 15 keV accelerating voltage, 20 nA beam current, and ca. 1 μm beam diameter. ZAF corrections (Yui and Aoki 1986) were made based on the end member formula $Mn^{3+}{}_6Mn^{2+}SiO_{12}$; the number of divalent elements (Mn^{2+}, Ca, Mg) is equal to the number of Silicon and the remaining manganese is in Mn^{3+} state.

The change of the cell parameters depending on the chemical composition could not be detected because of small size of grains and its zonal structure.

The chemical composition of rhodochrosite is shown in Table 1. The rhodochrosite is characterized by the high MgO contents in comparison with

Table 1. Analyses of rhodochrosite from Hikari Mine

	No.1	No.2	No.3	No.4	average
(wt%)					
$MnCO_3$	63.4	57.3	56.6	63.1	60.1
$MgCO_3$	20.8	18.1	13.2	22.5	18.6
$CaCO_3$	13.9	23.2	29.2	12.6	19.8
$FeCO_3$	0.2	0.0	0.1	0.1	0.1
total	98.3	98.6	99.2	98.3	98.6
(number of cations based on 3 Oxygens)					
Mn^{2+}	0.59	0.53	0.52	0.58	0.56
Mg^{2+}	0.26	0.23	0.17	0.28	0.23
Ca^{2+}	0.15	0.25	0.31	0.13	0.21
Fe^{2+}	0.00	0.00	0.00	0.00	0.00
total	1.0	1.0	1.0	1.0	1.0

rhodochrosites from other mines in the south west of Hokkaido.

The chemical compositions of braunite are shown in Table 2 with increase order of SiO_2 content. The CaO contents decrease gradually from 1.91 wt% to 1.56 wt% with increase of SiO_2 content. A scanning profile across an idiomorphic braunite grain is shown in Fig. 1. It is indicated that Silicon and magnesium contents increase with scanning the grain from the core to the rim of the grain. In Fig. 2, the number of magnesium and calcium ion and the sum of these are plotted against the number of Silicon ion based on 12 oxygens. The sum of magnesium and Ca ions (N_{Mg+Ca}) is related to that of silicon ions (N_{Si}) with the equation :

$$N_{Si} = 1.0106 \times N_{Mg+Ca} - 0.81855 , \quad R^2 = 0.837$$

(regression line of 9 analyses points),

where R^2 denotes a coefficient of correlation. The SiO_2 and MgO contents range from 9.92 wt% to 12.37 wt% and from 0.18 wt% to 1.95 wt%, respectively. The fact that the increasing ratio of divalent cations to SiO_2 component takes almost 1 suggests that the excess of silicon content is due to the solid solubility of the (Mg, Ca) SiO_3 component to braunite. Especially $MgSiO_3$ component is much effective for making the solid solution in this case.

The existence of a complete solid solution along the join $3Mn_2O_3 \cdot MnSiO_3$ - $3Mn_2O_3 \cdot MgSiO_3$ has been experimentally confirmed by Momoi (1982) and Reinecke et al.(1991). It should be noted however that the excess of Silicon does not occur in the above type of solid solution since the atomic ratio Si / (total cations) is maintained at 1/8.

From the chemical analysis data above mentioned it is estimated that the

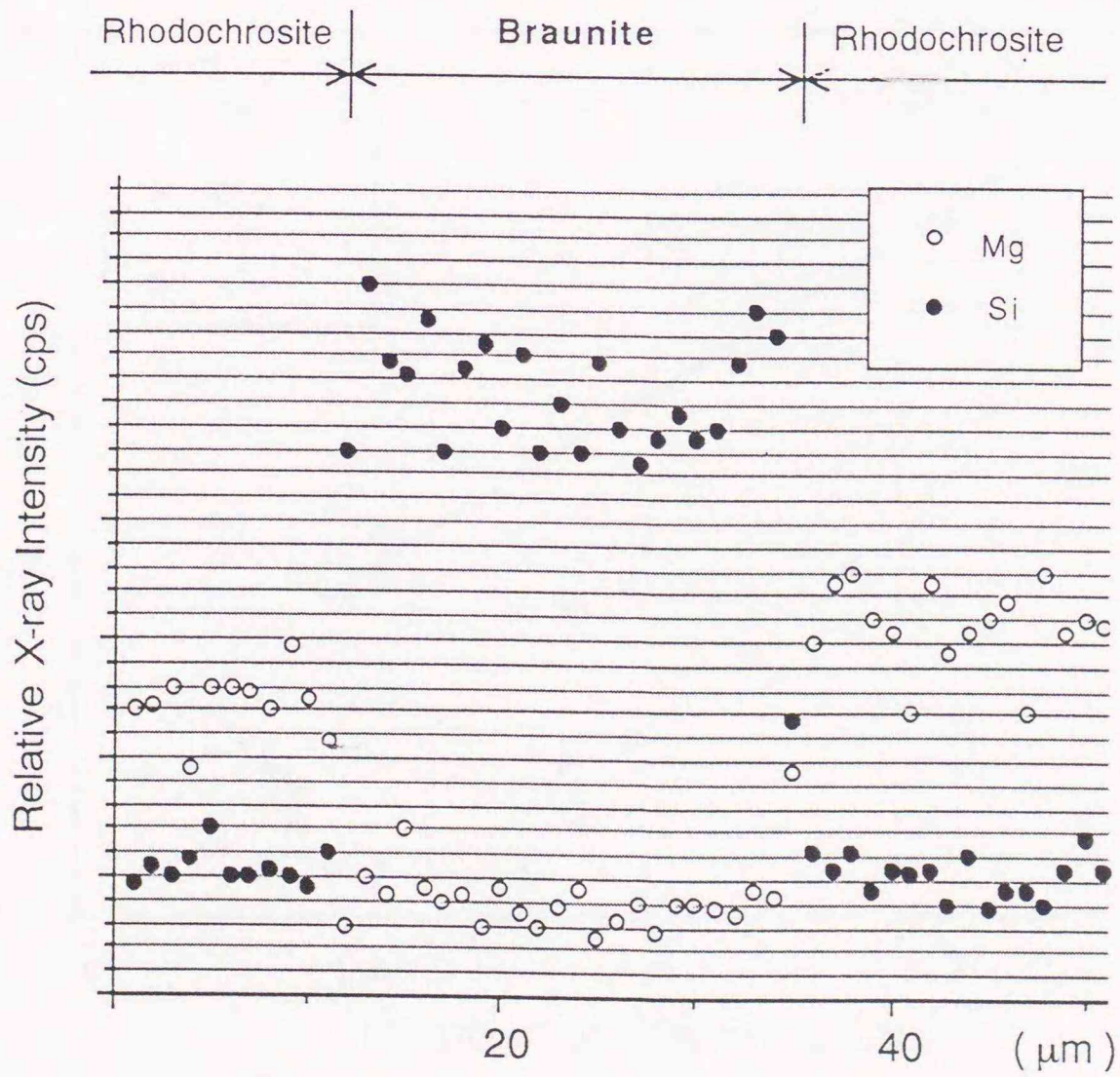

Fig. 1. X-ray line scanning analysis of ideomorphic braunite crystal. Outer zone of braunite is Mg-rich rhodochrosite. Beam diameter is ca. 1 μm. The figure shows that the amounts of Si and Mg are more at the rim of the braunite grain comparing with those in the inside of the grains.

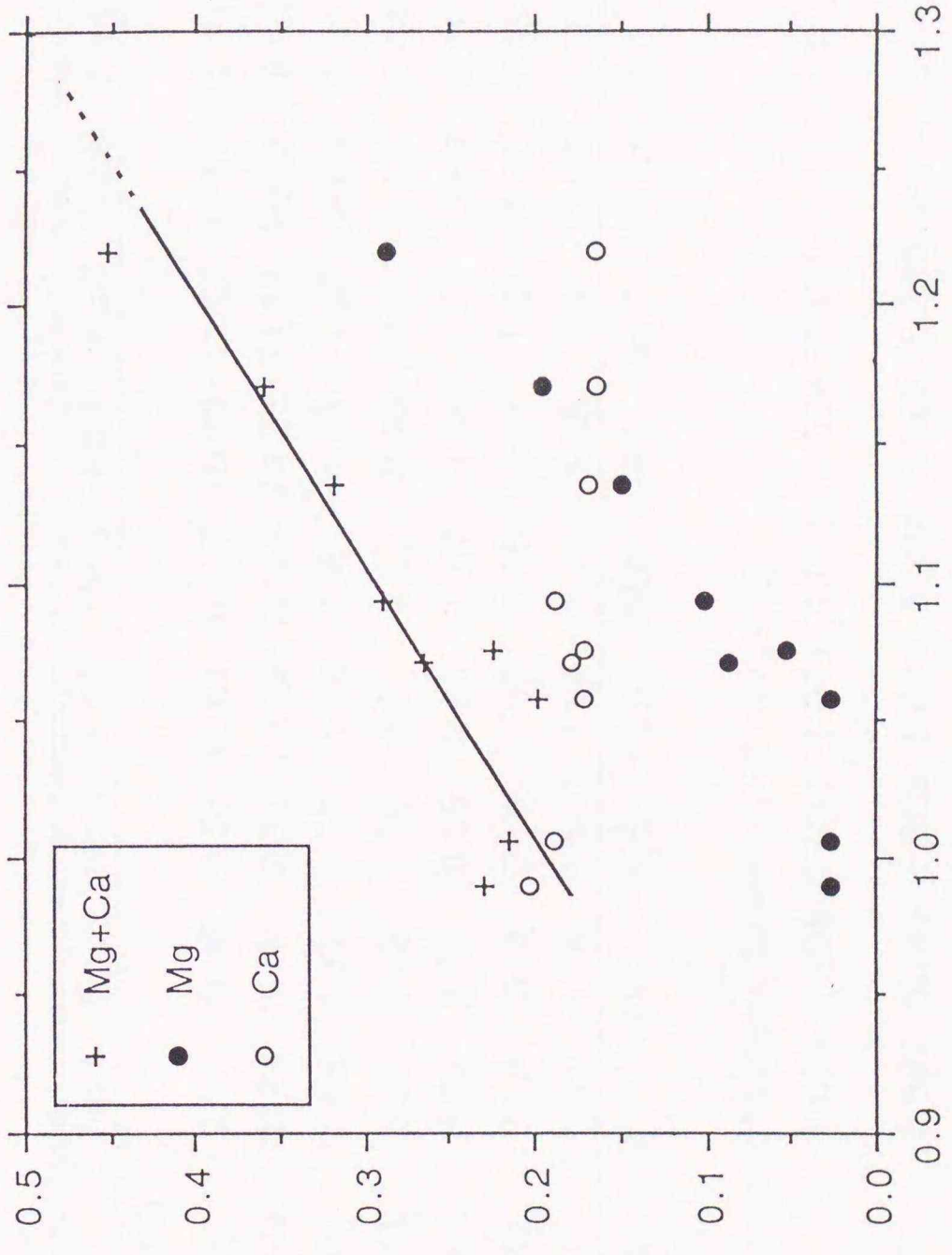

Fig. 2. Number of atoms of braunite based 12 oxygens. Solid line represents regression line of 9 analyses points. $N_{Mg+Ca} = 1.0106 \times N_{Si} - 0.81855$. Coefficient of correlation : $R^2 = 0.837$.

Table 2. Analyses of braunite from Hikari Mine

	No.1	No.2	No.3	No.4	No.5	No.6	No.7	No.8	No.9
(wt %)									
SiO_2	9.92	10.08	10.53	10.81	10.77	10.93	11.43	11.85	12.37
Mn_2O_3	76.24	75.64	72.91	74.28	72.66	73.23	71.17	70.72	68.63
Al_2O_3	1.65	1.77	1.73	1.65	1.47	1.43	1.62	2.09	2.00
Fe_2O_3	0.55	0.48	1.50	0.81	2.03	0.80	2.14	1.37	2.44
MnO	8.99	9.36	10.09	9.60	10.07	9.49	9.71	9.69	9.19
MgO	0.18	0.18	0.18	0.59	0.35	0.68	1.01	1.32	1.95
CaO	1.91	1.76	1.60	1.67	1.61	1.75	1.58	1.56	1.56
total	99.4	99.3	98.5	99.4	99.0	98.3	98.7	98.6	98.1
(number of cations based on 12 oxygens)									
Si	1.094	1.006	1.057	1.071	1.075	1.094	1.135	1.170	1.219
Mn^{3+}	5.582	5.743	5.569	5.604	5.524	5.582	5.380	5.314	5.149
Al	0.167	0.209	0.204	0.193	0.173	0.169	0.189	0.243	0.232
Fe	0.060	0.036	0.113	0.060	0.153	0.060	0.160	0.102	0.181
ΣM^{3+}	5.809	5.988	5.886	5.857	5.850	5.811	5.729	5.659	5.562
Mn^{2+}	0.805	0.791	0.857	0.806	0.852	0.805	0.817	0.811	0.767
Mg	0.102	0.027	0.027	0.088	0.052	0.102	0.150	0.195	0.287
Ca	0.188	0.188	0.172	0.178	0.172	0.188	0.168	0.165	0.164
ΣM^{2+}	1.095	1.006	1.056	1.072	1.076	1.095	1.135	1.171	1.218
total	8.00	8.00	8.00	8.00	8.00	8.00	8.00	8.00	8.00

excess of silicon content is related to the substitution of $2Mn^{3+} = Mg^{2+} + Si^{4+}$ forming a solid solution expressed as $(Mn^{3+}_{6-2x}Mg_xSi_x)Mn^{2+}SiO_{12}$ or $3Mn_2O_3 \cdot MnSiO_3$ - $3MgSiO_3 \cdot MnSiO_3$. The solid solubility of "$MgSiO_3 \cdot$" molecule in the ideal braunite phase $3Mn_2O_3 \cdot MnSiO_3$ were experimentally examined as described in the following chapters.

1 - 1 - 2 New occurrence of braunite II from Wafangy, China

Geological setting of Wafangy deposit

In the Wafangzi mine area, China, the manganese ore bearing middle part of the Tieling formation has a conformable lower contact with laminated dolostone and an unconformable contact with the overlying Cambrian conglomerates. The ore-bearing formation comprises a basal dolomitic conglomerate, shale, and an upper silty limestone. Three manganese ore bodies occur interstratified with shale that shows lateral change in color from reddish-brown to black. Locally, the ore bodies are lenticular in shape, showing pinch and swell structures, but are conformable with the host rock. Manganite is the major constituent of the ore hosted in red or brown shale whereas rhodochrosite and ferroan rhodochrosite constitute the ore hosted in black shale and black calcareous shale.

The Wafangzi manganese deposit was grouped under sedimentary ores of mudrock-hosted type. There are the Jiguanshan ore block, the Qujiagon ore block, the east and north hill sections of the Baoshenmio ore block. Braunite II were collected from Jiguanshan ore bodies which altered with granite intrusion. The mineral assemblages are braunite, braiuniteII, magnetite, jacobsite and

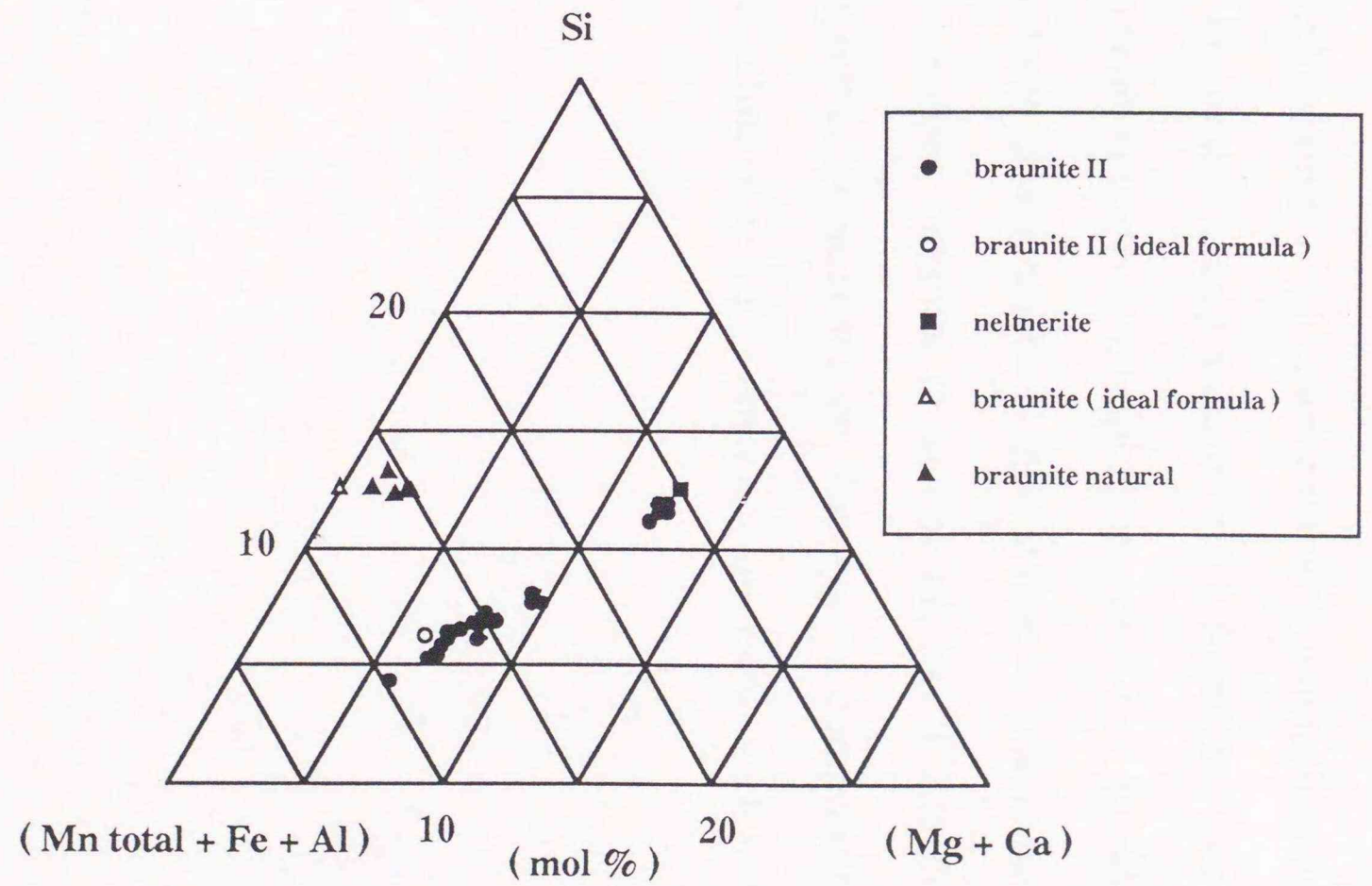

Fig. 3 Braunite II compositions from Wafangzi mine, China.

manganese hydro - silicate which have not identified yet. braunite and braunite II shows idiomorphic shape and around 10 μm in diameter. Chemical compositions of braunite II and coexisting braunite, neltnerite are listed in Table 3. Fig. 3 shows that the compositional variations of braunite, braunite II and neltnerite solid solutions on the silicon - sum of total manganese and trivalent cations (iron and aluminium) - divalent cations (magnesium and calcium). Compositions of braunite II solid solution vary from the ideal braunite II composition to ideal neltnerite composition and not to ideal braunite composition. From these data, it can be suggested that the possibility of existence of solid solution between braunite II and neltnerite. These compositional relationships are observed at the first time. This type of compositional variation in braunite II solid solution seems to have a relationship with that of Si - rich braunite.

Table 3. Compositions of Braunite II

	5	6	13	14	15	16	17	18	19	20
(wt %)										
MgO	0.5	0.9	0.7	0.7	0.6	0.7	0.7	0.9	0.7	0.7
CaO	16.3	3.7	5.0	4.7	4.3	6.7	4.3	4.0	4.9	4.2
Mn2O3	56.1	71.6	75.4	75.9	76.4	73.3	74.3	75.6	76.6	75.6
Fe2O3	9.8	18.1	12.5	12.1	13.3	12.1	15.2	14.4	12.5	14.4
Al2O3	0.6	0.9	0.7	0.7	0.5	0.4	0.4	0.5	0.4	0.5
SiO2	4.4	4.2	5.7	5.4	5.0	5.0	4.9	4.3	5.4	4.6
TOTAL	87.7	99.4	100.0	99.5	100.2	98.2	99.7	99.6	100.5	99.9
(O = 24)										
Mg	0.16	0.28	0.20	0.20	0.19	0.22	0.20	0.27	0.21	0.21
Ca	4.07	0.81	1.09	1.03	0.93	1.49	0.94	0.87	1.05	0.91
	4.23	1.09	1.28	1.23	1.12	1.71	1.14	1.14	1.25	1.12
Mn	9.92	11.14	11.54	11.70	11.75	11.50	11.50	11.75	11.73	11.69
Fe	1.72	2.79	1.89	1.85	2.03	1.88	2.32	2.21	1.89	2.20
Al	0.16	0.21	0.18	0.16	0.11	0.10	0.10	0.11	0.08	0.11
	11.81	14.13	13.60	13.71	13.89	13.48	13.92	14.07	13.70	14.00
Si	1.02	0.86	1.15	1.10	1.02	1.03	0.99	0.88	1.09	0.94
TOTAL	17.06	16.08	16.03	16.03	16.02	16.22	16.05	16.09	16.05	16.06

1 - 2 Experiments

1 - 2 - 1 Experimental method

The phase equilibria related to braunite phases were examined at 1100 °C in air in the pseudo-ternary system $MnSiO_3$ - $MgSiO_3$ - Mn_2O_3 as shown in Fig. 4. In the diagram, compositions with the ideal atomic proportion of silicon in braunite lies only along the join $3Mn_2O_3 \cdot MnSiO_3$ - $3Mn_2O_3 \cdot MgSiO_3$. The compositions with an excess of silicon due to the solid solubility of "$3MgSiO_3 \cdot MnSiO_3$" molecule to the ideal phase $3Mn_2O_3 \cdot MnSiO_3$ are shown by the dashed line which reaches to the join $MgSiO_3$ - $MnSiO_3$ at the composition $3MgSiO_3 \cdot MnSiO_3$.

As starting materials, reagent grade MnO_2 (pyrolusite), MgO (periclase) and SiO_2 (quartz) were weighed in desired proportions and mixed in an agate mortar under ethanol. The specimens were put into a platinum crucible at 1100 °C in open air furnace for 24 hours and then cooled by removing the crucible from the furnace. The specimens were examined by X-ray powder diffraction using a graphite monochromated diffractometer with Ni-filtered CuKα radiation. When reactions were not completed, the specimens were powdered and reheated repeatedly until the final products were in phase equilibrium. The initial products were mixture of braunite, hausmannite and quartz. Then hausmannite and quartz reacted to braunite or braunite and tephrite. It took maximum 23 days to reach phase equilibrium.

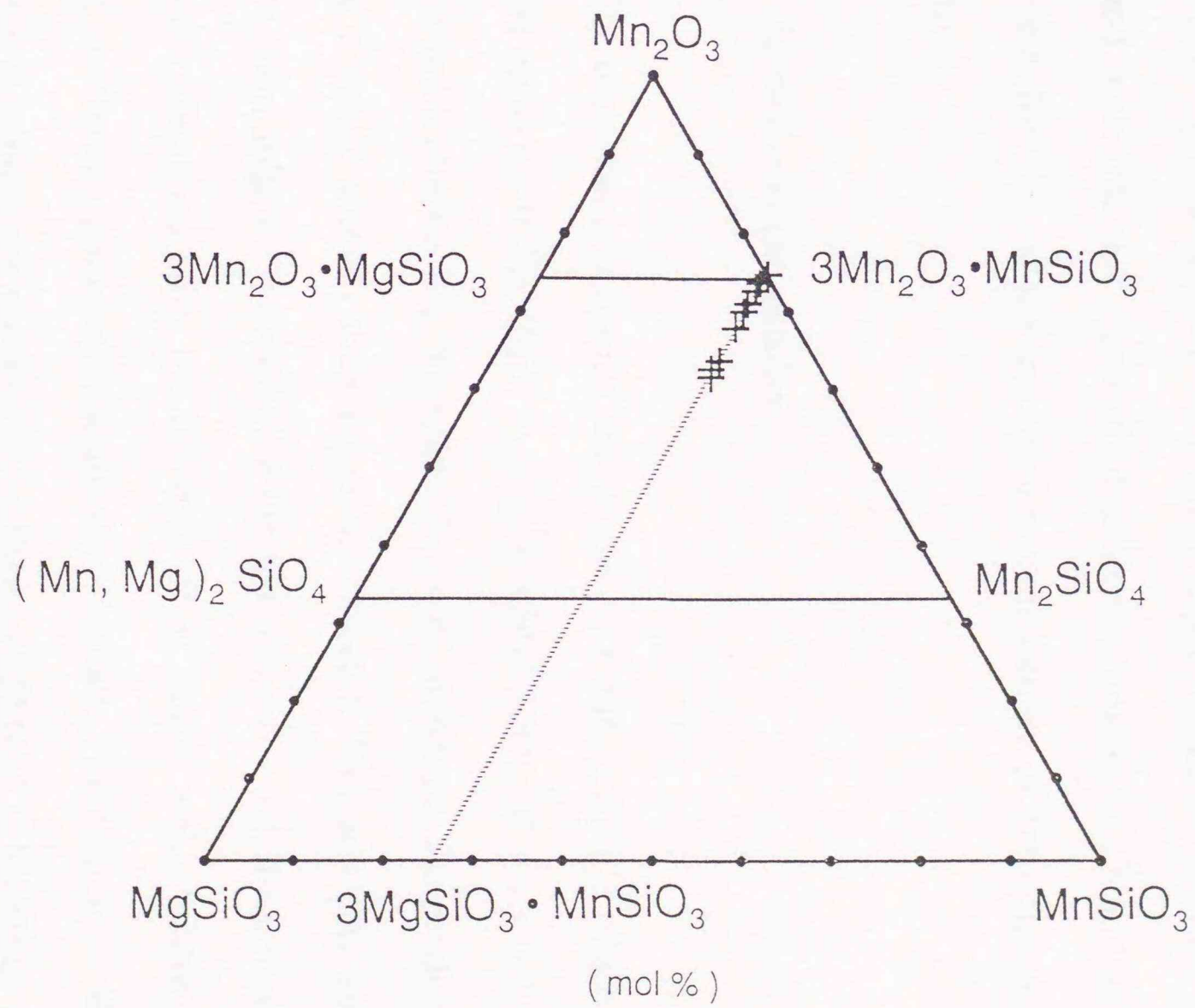

Fig. 4. Composition of starting materials on the pseudo-ternary system Mn_2O_3 - $MnSiO_3$ - $MgSiO_3$.

1 - 2 - 2 Determination of cell parameters

The lattice parameters of final phase were refined by the least squares method using the X-ray diffraction data. Reflection patterns were measured with scanning step speed of 0.01 degree per 3 seconds and 2θ angles were corrected with internal standard of silicon. Number of 17 and 15 reflections were used for the lattice parameters calculation of braunite and tephroite respectively.

1 - 3 Experimental results

The experimental results are shown in Table 4. Single phase of braunite appeared up to x = 0.2 of $(Mn^{3+}_{6-2x}Mg_xSi_x)\cdot Mn^{2+}SiO_{12}$. For x > 0.2, two phases, braunite and tephroite $(Mn,Mg)_2SiO_4$, were obtained. All the products were fine grained crystals smaller than 1 μm in diameter. The unit cell parameters of braunite solid solution are shown in Fig.5. For x = 0 ~ 0.2, the lattice parameters of *a* and *c* decrease with the increase of x. For x > 0.2 where two phases coexist, the lattice parameters maintain constant. The change of the slopes at about x = 0.2 indicates the solubility limit of "$3MgSiO_3\cdot MnSiO_3$" molecule to the ideal braunite at 1100 °C in air. The composition x = 0.2 corresponds to 12.16 wt% SiO_2. One might argue for that the change of lattice parameters can be explained by the substitution of magnesium ion for divalent manganese ion without incorporation of silicon ion. The change of lattice parameters by the

latter type substitution (Momoi et al., ibid.) are shown in Fig. 6 for comparison. It is evident from Fig. 6 that the present result is different from their data.

The lattice parameters of tephroite associated with braunite are almost constant for No.6 ~ No.9 starting composition (Table 5). The compositions of tephroite are estimated as $(Mn_{1.3}Mg_{0.7})SiO_4$ from the experimental data of the system Mg_2SiO_4 - Mn_2SiO_4 by Nishizawa (1972). The above composition corresponds well with the composition, $(Mn_{1.375}Mg_{0.625})SiO_4$, of the point, where the two joins $3Mn_2O_3 \cdot MnSiO_3$-$3MgSiO_3 \cdot MnSiO_3$ and Mg_2SiO_4-Mn_2SiO_4 crosses in Fig. 4.

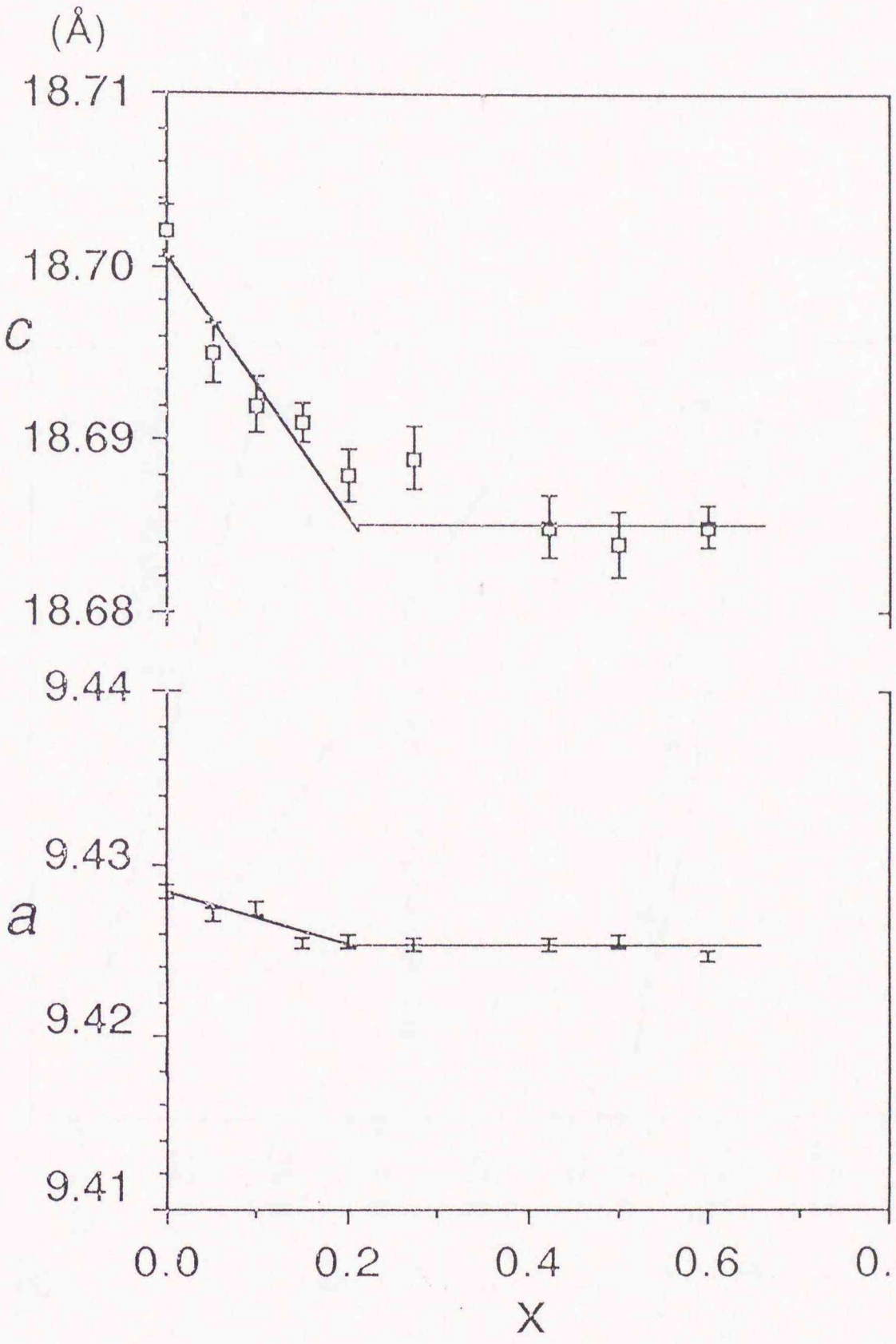

Fig. 5. Composition dependence of the unit cell parameters of Si - rich braunite.

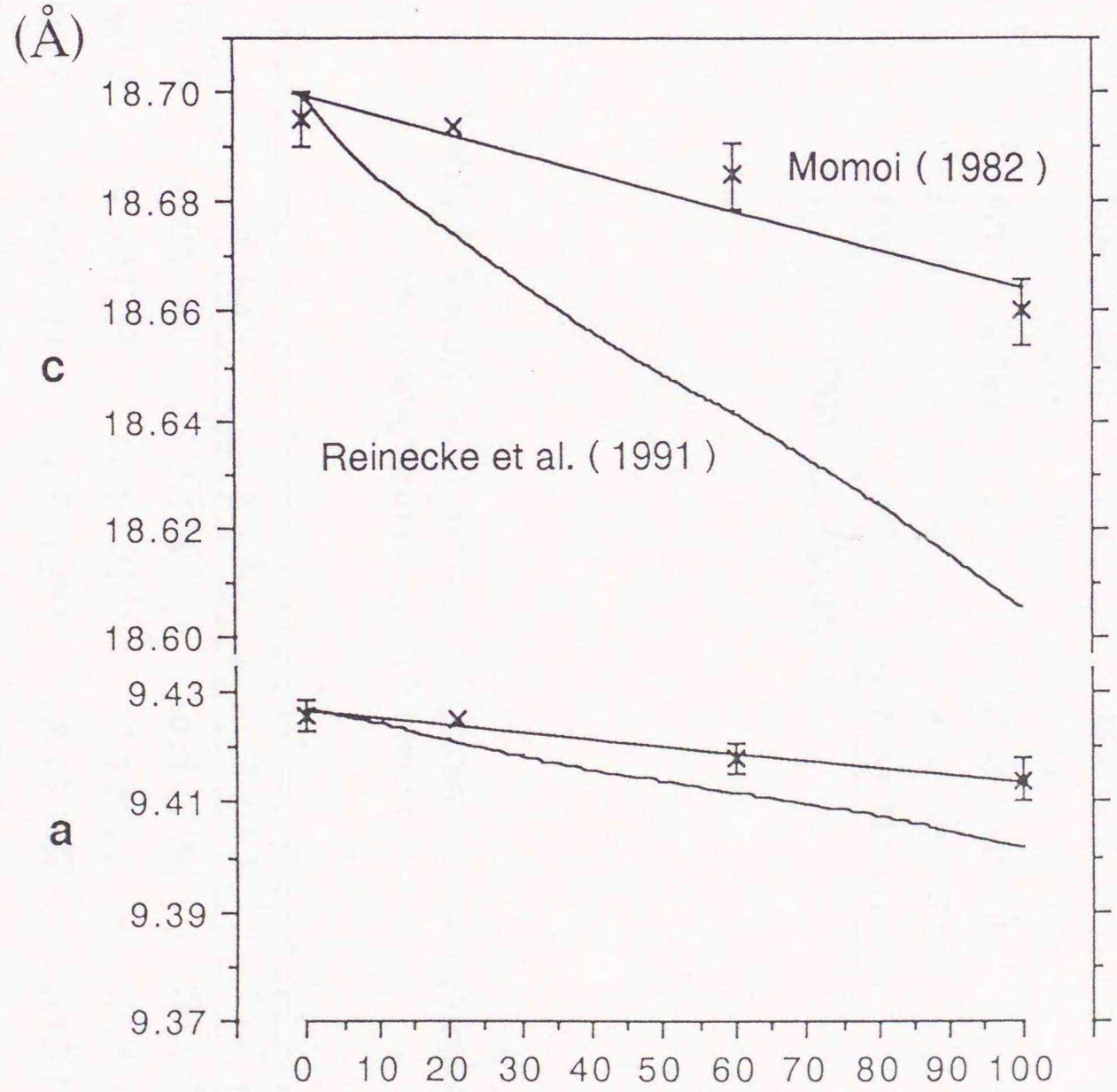

Fig. 6 Variations of lattice parameters depending on the Mg substitution in the divalent site of braunite determined by Momoi (1982) and Reinecke et al., (1991).

Table 4. Starting materials and run products.

	X	Duration (days)	Products
No.1	0.0	12	braunite
No.2	0.05	23	braunite
No.3	0.1	23	braunite
No.4	0.15	23	braunite
No.5	0.2	20	braunite
No.6	0.275	23	braunite, tephroite
No.7	0.425	23	braunite, tephroite
No.8	0.5	20	braunite, tephroite
No.9	0.6	23	braunite, tephroite

X : $Mn^{2+}(Mn^{3+}_{(6-2X)}Mg_XSi_X)SiO_{12}$

Table 5. Variations of the unit cell parameters of tephroite coexisting with Si - rich braunite

	a (Å)	*b* (Å)	*c* (Å)	V (Å^3)
No.6	4.851(6)	10.510(6)	6.177(9)	315.0(6)
No.7	4.837(2)	10.512(4)	6.176(3)	314.1(2)
No.8	4.835(1)	10.512(2)	6.171(2)	313.6(1)
No.9	4.843(1)	10.516(1)	6.177(1)	314.6(1)

1 - 4 Discussion

It becomes clear from our experiments that the substitution $2Mn^{+3} = Mg^{+2} + Si^{+4}$ can be possible in braunite structure and this substitution cause the decrease of cell constants (especially *c* axis). From the comparison of ion radii between Mn^{+3} (0.66) and the mean of Mg^{+2} and Si^{+4} (0.57) (Whittaker et al., 1970), this decreasing trend is explicable. According to Moore and Araki (ibd.), braunite structure is constructed with three kinds of octahedrally coordinated Mn^{3+} site; two in the *A* sheet and another in the *B* sheet. Thus the silica excess phase of the present study could be explained by extending the stacking algorithm of de Villiers and Buseck (ibid.) to include the stacking sequence such as [*BB*], without forming the solid solution of $2Mn^{+3} = Mg^{+2} + Si^{+4}$. If it happened, some disordered stacking sequences of *A* and *B* layers along the *c* axis had to be observed. But we did not observed any diffuse (0 0 l) reflections in the X-ray diffraction pattern at all. The smooth decrease of *c* parameter with increasing *x* as seen in Fig. 5.can be rather explained by the presence of solid solution, $(Mn^{3+}_{6-2x}Mg_xSi_x)\cdot Mn^{2+}SiO_{12}$. In the latter case, the substitution $2Mn^{3+} = Mg^{+2} + Si^{+4}$ should occur at random Mn^{3+} sites in the ordered braunite structure of $[AB]_4$, possibly in the *A* layers. Consequently, some oxygens must be shifted to create a cubic coordination for magnesium and a tetrahedral coordination for Silicon, if the octahedral coordination for Si^{+4} are not favoured. Additionally, the fact that the almost constant calcium contents over all analysis points are nearly constant with the increase of silicon and magnesium contents (Fig. 2) may suggest that there are no change of frequency

of *B* layers in the braunite structure. Because calcium ions locate only at *B* layers not at *A* layers, stacking sequence $[AB]_4$ must be changeless in this case.

On the other hand, decrease of cell parameters could also be explained by the substitution of magnesium to manganese ions in divalent cations sites. Tephroites in the products have almost constant composition $(Mn_{1.3}Mg_{0.7})\ SiO_4$, and hence it is difficult to consider that the change of cell parameters are caused by the substitution within the divalent site.

The formation of Mg - rich tephroite on the join $3Mn_2O_3{\cdot}MnSiO_3$ - $3MgSiO_3{\cdot}MnSiO_3$ demands reduction of some Mn^{3+} ions to Mn^{2+} state, and hence, the solid solubility of "$3MgSiO_3{\cdot}MnSiO_3$" molecule in braunite may increase with the increase of f_{O_2} at a constant temperature. It should be noted that the stable silica excess phase coexisting with braunite at 1100 ˚C in air is tephroite in this study, instead of rhodonite as reported by Abs-Wurmbach et al., (1983) in the Mn-Si-O system. It will be reasonable to suppose that the upper limit of oxygen fugacity which can stabilize a phase $(Mg,Mn)_2SiO_4$, decreases with increase of the tephroite component in the phase at a constant temperature.

Although the temperature chosen in the present experiment is much higher than those for formation of natural braunite, the experimental results well explained the analyses data of braunite from Hikari mine. The Si - rich braunite from Hikari mine have been formed at the cost of high Mg-rhodochrosite, since magnesium content of braunite is high at the rim of the crystal making a zonal structure.

Braunite shows the solid solubility to the neltnerite composition, not to the braunite II composition and braunite II shows that to neltnerite, not to braunite

as showen in Fig. 3. From the comparison of these compositional variations of braunite II with that of braunite and neltnerite, It seems realistic that the substitutions of calcium and silicon for manganese between neltnerite and braunite II is related to the layer stacking variation of *A'* and *B* sheet, because the compositions of braunite II solid solution keep the constant ratio of silicom and divalent cations, Si : (Mg + Ca) = 1.

Otherwise, the substitution of calcium between braunite and neltnerite caused by the interlayer substitutions in the *B* sheet keeping constant SiO_2 contents.

1 - 5 Conclusions

It becomes clear from the experiments that the substitution $2Mn^{+3} = Mg^{+2} + Si^{+4}$ can be possible in braunite structure and this substitution causes the decrease of cell constants (especially *c* axis). It may be reasonable that the substitution is related to the inter layer variations of substitution and not to the stacking variations of the layers.

Part 2 - pyroxenoids

2-0 Introduction

A variety of manganese silicates of the $RSiO_3$ type are common constituents of the Mn silicate-carbonate rocks, metamorphosed from the greenschist to the granulite facies. In the natural occurrences, the most abundant $RSiO_3$ type of pyroxenoid phases are rhodonites, pyroxmangites, wollastonites and bustamites. Compatibility relations between these phases and the Mn bearing pyroxenes have been inferred from the compositions of the natural phases in the $MnSiO_3$-$CaSiO_3$-$FeSiO_3$, $MnSiO_3$-$MgSiO_3$-$CaSiO_3$ (Brown et al., 1980) and $MnSiO_3$-$MgSiO_3$-$FeSiO_3$ (Petersen et al., 1984) faces of the $RSiO_3$ tetrahedron.

Considerable experimental works have been carried out on the stability of pyroxenoids and the associated $RSiO_3$ phases along the join $MnSiO_3$-$MgSiO_3$ (Ito, 1972; Momoi, 1973; Iwabuchi & Hariya ,1985; Huebner, 1986), $MnSiO_3$-$CaSiO_3$ (Momoi, 1968; Abrecht & Peters, 1975, 1980; Kakuda et al., 1991), Fe-rich end of the join $FeSiO_3$-$MnSiO_3$ (Bohlen et al., 1980a), MnO-MgO-FeO-SiO_2-CO_2 (Banerjee et al., 1988) and $CaSiO_3$-$FeSiO_3$-$MnSiO_3$-(Ca, Fe, Mn)Cl_2-H_2O (Ogino et al., 1992) at different pressures and temperatures. Polymorphism of $MnSiO_3$ was studied by Akimoto & Syono (1972), Momoi (1974) and Maresch & Mottana (1976). They showed that pyroxmangite of $MnSiO_3$ composition is the high pressure, low temperature polymorphic transformation with respect to rhodonite of the same composition. These previous works show that the stability fields of pyroxenoids change with pressure and temperature.

The coexisting pyroxmangite and rhodonite pairs in natural occurrences

represent the mutual solubility limits of major elements in the two phases, and the composition of the miscibility gap, as well as the pyroxenoid compositions, depends on P-T conditions.

Natural pyroxenoids and Mn-pyroxenes generaly contain $MnSiO_3$, $MgSiO_3$, $CaSiO_3$ and $FeSiO_3$ components. In order to elucidate the stability of Mn-pyroxenoid, it is important to determine the effect of the Mg, Ca and Fe on the stability of these $RSiO_3$ phases. However, experimental study using multicomponent system is very complicated and it requires a number of runs.Therefore ternaly system Mn - Mg - Ca without Fe was sellected in this study. There are no published data on the stability fields of pyroxenoids and pyroxenes in the system $MnSiO_3$-$MgSiO_3$-$CaSiO_3$ which represents some Fe-poor natural system. In this paper we present the experimental data on the phase relationship of Mn-rich portion in the ternary system of $MnSiO_3$-$MgSiO_3$-$CaSiO_3$ at several P-T conditions. The experiments conducted at pressure and temperature conditions corresponding to normal crustal metamorphism throw considerable light on the forming condition of Fe-poor (Mn-Mg-Ca)SiO_3 pyroxenoid and pyroxene minerals.

The present experiments were designed to get the the temperature and pressure dependence of the composition of coexisting pyroxenoid solid solusiosn in the ternary system, and to test the possibility of using such assemblages as geothermometer.

2-1 General Properties of Mn pyroxenoids

2-1-1 Crystal structures of pyroxenoids

The Mn - rich pyroxenoids are single - chain silicates that constitute a polysomatic series. The pyroxenoid polysomatic series is based on the stacking of pyroxene - like (P) and wollastonite - like (W) structural slabs parallel to (1 1 -1) of pyroxene, and includes the Mn - rich pyroxenoid minerals, rhodonite (PW) and pyroxmangite (PPW) (Thompson, 1978; Angel and Burnham, 1991; Veblen, 1991).

The various structures of pyroxenoids also differ in the periodicity of the tetrahedral chain and in the corresponding arrangement of the octahedrally coordinated cations. In this manner they constitute a structural series that has been classified according to the number n of the tetrahedra between offsets that interrupt pyroxene - like configurations (Liebau, 1962). Then rhodonite and pyroxmangite are represented as n = 5 and 7, respectively. Bustamite, another three - repeat pyroxenoid, is based on a different linkage of the octahedral and tetrahedral layers, and therefore is not a member of this series (Koto, 1976; Thompson, 1978).

2-1-2 Natural occurrences and previous works

Rhodonite - pyroxmangite assemblages from different localities are listed in Table 6 and summarized in Figure 7. The data from Buritirama (Brazil) are taken from Peters (1977), Koduru (north-eastern part of Andhra Pradesh, India) from Sivaprakash (1980) and Bald Knob (North calolina, U.S.A) from Winter et al. (1981).

In the Buritirama mine, the mineral assemblages in the rocks associated

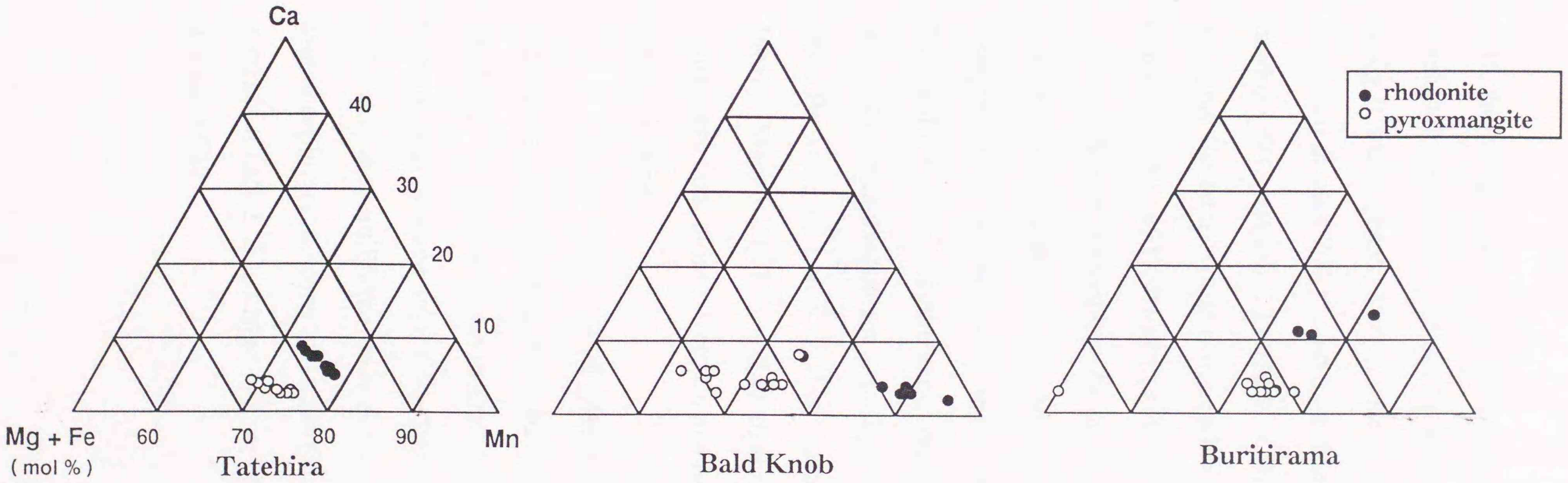

Fig. 7 Triangular composition diagram showing the coexisting rhodonite and pyroxmangite pairs of the natural samples. Filled circle represents rhodonite and open circle represents pyroxemangite. References are in the literature.

with the manganese - protores indicate a metamorphism in the lower to middle amphibolite facies and assumed a temperature is 550 ˚C ± 50 ˚C, and total pressure is 3 ± 0.3 kb (Peters, 1977). The peak metamorphic condition of Kodulu mine is estimated at least 700 ˚C and 6 kb from the compositions of coexisting manganese oxides (Sivaprakash). Pressure of Bald Knob mine was estimated to be as 5 kb applying the temperature using carbonats stability field to the kyanite - sillimanite phase boundary of Holdway (1971) by Winter et al. (1981).

Natural rhodonite - bustamite assemblages from different localities were investigated and analyzed in previous works (Table. 7). Figure 8 shows the compositional variations of these assemblages.The manganese deposit from Ravinella di Sotto (Ivrea zone, Northern Itary) and especially the rhodonite - bustamite assemblages are described in detail in Abrecht et al. (1979). The data from Broken Hill (N. S. Wales, Australia) are taken from the papers of Binns (1968), Mason (1973) and Hodgson (1975). Andhra Pradesh (Eastern Ghat manganese belt, India), from Bhattacharyya (1986) and Hoskins (Australia) from Ashley. (1989).

Abrecht et al. (1979) obtained 620 ˚C as the blocking temperature during cooling of Ravinella di Sotto mine by comparing the miscibility gap in the system $MnSiO_3$ - $CaSiO_3$ with the natural data. Hodgson suggested that Broken Hill mine was metamorphosed under the hornblende granulite facies. Abrecht (1980) estimated the equilibrium temperature of Broken Hill mine to be 500 - 550 ˚C. Metamorphic conditions of Hoskins mine are estimated to be a middle to upper greenshist facies. The range is T = 450 - 500 ˚C, P < 4 kb (probably < 2 kb) (Ashley, 1989).

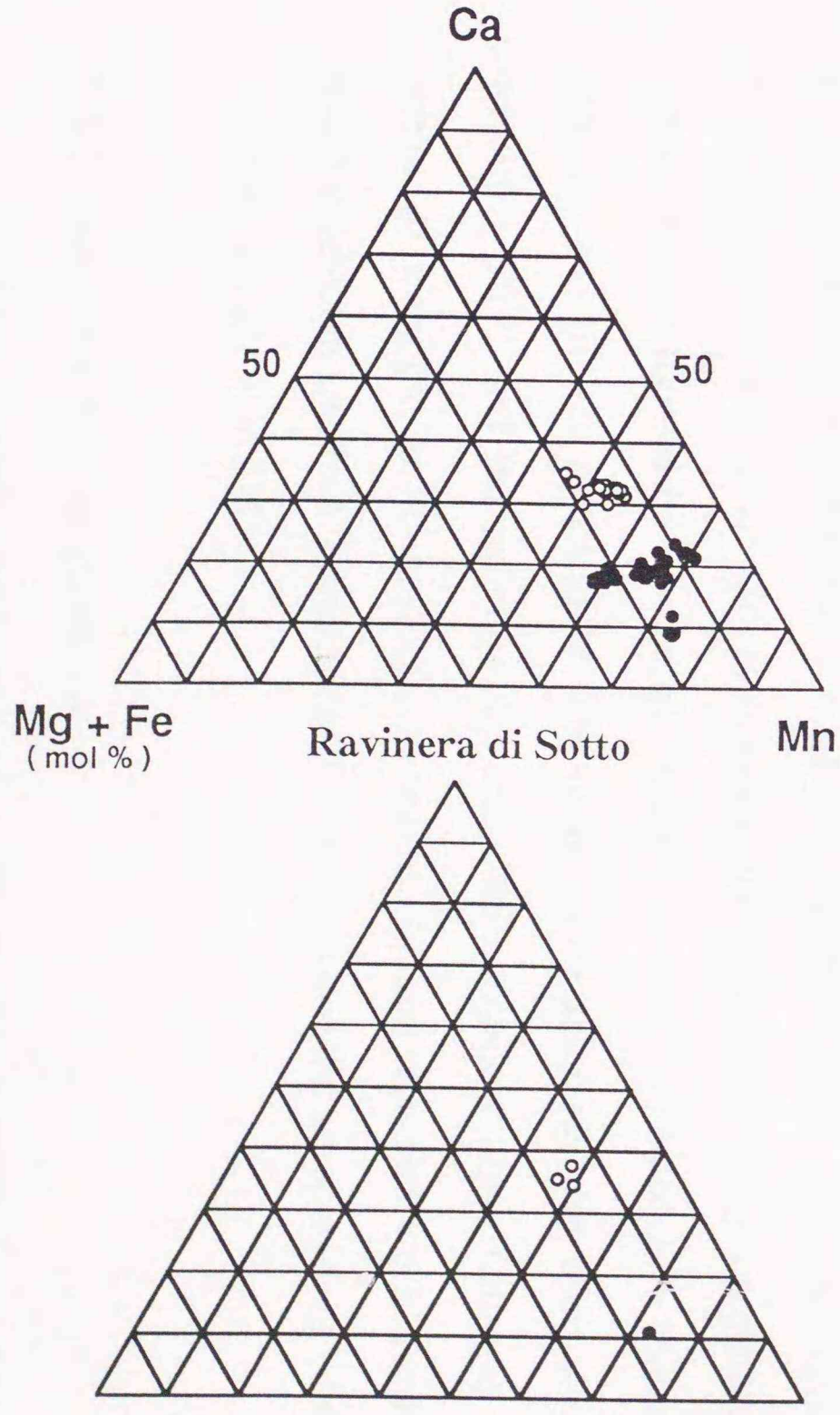

Ravinera di Sotto

Broken Hill

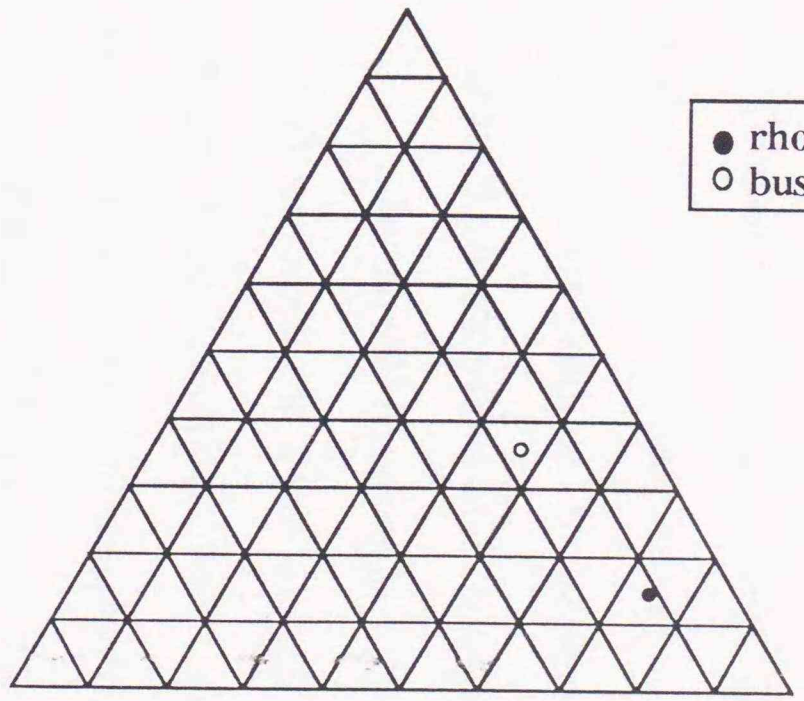

Hoskins

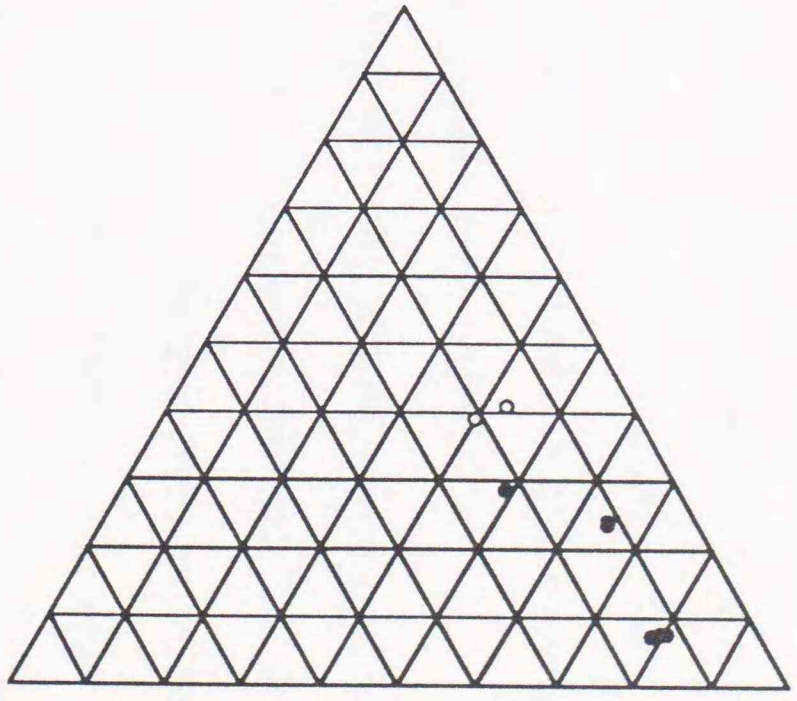

Andhra Pradesh

Fig. 8 Triangular composition diagram showing the coexisting rhodonite and bustamite pairs of the natural samples. Filled circle represents rhodonite and open circle represents bustamite. References are in the literature.

2-2 Experiments

2-2-1 Experimental method

Two types of starting material were used for the experiments ; Oxide mixtures of reagent grade MnO_2, SiO_2, MgO and CaO, and pyroxenoid mixture of rhodonite $MnSiO_3$, pyroxmangite $(Mn_{0.5}Mg_{0.5})$ SiO_3 and bustamite $(Mn_{0.5}Ca_{0.5})$ SiO_3 that were produced by heating at 1200°C in air. These mixtures were weighed in desired compositions and mixed in agate mortar under ethanol.

In the experiments at 1200°C in air, the charges (oxide mixtures) were put in a Pt crucible for 24hr and then cooled by removing the crucible from the furnace. When reactions were not complete, the charges were powdered and reheated repeatedly until the products were in phase equilibrium. The experiments at total pressure of 2 kbar were done with a cold-seal type hydrothermal apparatus. Temperature was measured with chromel-almel thermocouples. Temperature fluctuations were nearly ± 5 °C in long runs. Charges (pyroxenoid mixtures) were put in Au capsule with water as a catalyzer and sealed. High pressure experiments over 2 kb were carried out with piston cylinder apparatuses using the pressure cell similar to that figured by Hariya and Kennedy (1968). The pressure transmitting medium was molten pyrex glass. The temperature accuracy was estimated to be within ± 10°C and the pressure accuracy was within 1 kbar. Charges (oxide mixtures) were put in Pt capsules and sealed. All the capsules were checked for possible leakage after run. Experimental conditions and the compositions of starting materials are given in Table 6.

2-2-2 Analyses of run products

All the products were examined with an optical microscope and X-ray

Table 6 Compositions of starting materiels, run conditions and experimental results. Compositions of starting materials are represented in chemical formula of pyroxenoids as $RSiO_3$.

700°C, 1 kb

No.	Composition of starting materials	Run duration (days)	Products
#7	$MnSiO_3$	8	rhodonite
#8	$(Mn_{0.9}\ Mg_{0.1})SiO_3$	10	rhodonite
#9	$(Mn_{0.9}\ Ca_{0.1})SiO_3$	10	rhodonite + tr. bustamite
#1	$(Mn_{0.75}\ Mg_{0.25})SiO_3$	7	pyroxmangite + rhodonite
#2	$(Mn_{0.75}\ Mg_{0.2}\ Ca_{0.05})SiO_3$	8	rhodonite
#3	$(Mn_{0.75}\ Mg_{0.15}\ Ca_{0.1})SiO_3$	8	rhodonite + tr. bustamite
#4	$(Mn_{0.75}\ Mg_{0.1}\ Ca_{0.15})SiO_3$	8	rhodonite + bustamite
#6	$(Mn_{0.75}\ Ca_{0.25})SiO_3$	8	rhodonite + bustamite
#14	$(Mn_{0.7}\ Mg_{0.3})SiO_3$	8	pyroxmangite + rhodonite
#30	$(Mn_{0.7}\ Mg_{0.25}\ Ca_{0.05})SiO_3$	7	rhodonite + pyroxmangite
#31	$(Mn_{0.7}\ Mg_{0.2}\ Ca_{0.1})SiO_3$	7	rhodonite + bustamite
#12	$(Mn_{0.66}\ Mg_{0.3}\ Ca_{0.04})SiO_3$	9	pyroxmangite
#27	$(Mn_{0.6}\ Mg_{0.4})SiO_3$	8	pyroxmangite
#28	$(Mn_{0.6}\ Mg_{0.35}\ Ca_{0.05})SiO_3$	8	pyroxmangite + rhodonite
#29	$(Mn_{0.6}\ Mg_{0.3}\ Ca_{0.1})SiO_3$	8	rhodonite + pyroxmangite + bustamite
#21	$(Mn_{0.6}\ Mg_{0.25}\ Ca_{0.15})SiO_3$	10	rhodonite + pyroxmangite + bustamite
#19	$(Mn_{0.6}\ Mg_{0.2}\ Ca_{0.2})SiO_3$	11	bustamite + rhodonite
#16	$(Mn_{0.56}\ Mg_{0.4}\ Ca_{0.04})SiO_3$	9	pyroxmangite
#B	$(Mn_{0.5}\ Mg_{0.5})SiO_3$	8	kanoite
#26	$(Mn_{0.5}\ Mg_{0.45}\ Ca_{0.05})SiO_3$	8	pyroxmangite
#22	$(Mn_{0.4}\ Mg_{0.4}\ Ca_{0.2})SiO_3$	10	kanoite + bustamite
#23	$(Mn_{0.4}\ Mg_{0.3}\ Ca_{0.3})SiO_3$	10	kanoite + bustamite
#24	$(Mn_{0.4}\ Mg_{0.2}\ Ca_{0.4})SiO_3$	10	kanoite + bustamite
#25	$(Mn_{0.36}\ Mg_{0.6}\ Ca_{0.04})SiO_3$	12	kanoite
#101	$(Mn_{0.75}\ Ca_{0.25})SiO_3$	8	rhodonite + bustamite
#102	$(Mn_{0.9}\ Ca_{0.1})SiO_3$	40	rhodonite
#106	$(Mn_{0.75}\ Mg_{0.25})SiO_3$	39	rhodonite + pyroxmangite
#107	$(Mn_{0.55}\ Mg_{0.45})SiO_3$	30	kanoite + pyroxmangite

tr. : trace.

(Table 6)

700 °C 4 kbar

#8	$(Mn_{0.9}$	$Mg_{0.1}$		$)SiO_3$	8	rhodonite
#9	$(Mn_{0.9}$	$Ca_{0.1}$		$)SiO_3$	8	rhodonite + tr. bustamite
#1	$(Mn_{0.75}$	$Mg_{0.25}$		$)SiO_3$	5	pyroxmangite
#2	$(Mn_{0.75}$	$Mg_{0.2}$	$Ca_{0.05}$	$)SiO_3$	6	rhodonite + tr. pyroxmangite
#3	$(Mn_{0.75}$	$Mg_{0.15}$	$Ca_{0.1}$	$)SiO_3$	5	rhodonite
#4	$(Mn_{0.75}$	$Mg_{0.1}$	$Ca_{0.15}$	$)SiO_3$	3	rhodonite + bustamite
#30	$(Mn_{0.7}$	$Mg_{0.25}$	$Ca_{0.05}$	$)SiO_3$	8	pyroxmangite + rhodonite
#31	$(Mn_{0.7}$	$Mg_{0.2}$	$Ca_{0.1}$	$)SiO_3$	8	rhodonite + pyroxmangite
#28	$(Mn_{0.6}$	$Mg_{0.35}$	$Ca_{0.05}$	$)SiO_3$	6	pyroxmangite + tr. rhodonite
#29	$(Mn_{0.6}$	$Mg_{0.3}$	$Ca_{0.1}$	$)SiO_3$	6	pyroxmangite + rhodonite + tr. bustamite
#19	$(Mn_{0.6}$	$Mg_{0.2}$	$Ca_{0.2}$	$)SiO_3$	10	rhodonite + pyroxmangite + bustamite
#26	$(Mn_{0.5}$	$Mg_{0.45}$	$Ca_{0.05}$	$)SiO_3$	5	pyroxmangite + kanoite
#102	$(Mn_{0.9}$	$Ca_{0.1}$		$)SiO_3$	8	rhodonite + tr. pyroxmangite
#104	$(Mn_{0.85}$	$Mg_{0.15}$		$)SiO_3$	12	rhodonite
#105	$(Mn_{0.8}$	$Mg_{0.2}$		$)SiO_3$	10	rhodonite + pyroxmangite
#107	$(Mn_{0.45}$	$Mg_{0.55}$		$)SiO_3$	16	kanoite + pyroxmangite
#109	$(Mn_{0.8}$	$Ca_{0.2}$		$)SiO_3$	12	rhodonite + bustamite

tr. : trace.

(Table 6)

1000 °C 4 kbar

#8	$(Mn_{0.9}$	$Mg_{0.1}$		$)SiO_3$	6	rhodonite
#9	$(Mn_{0.9}$	$Ca_{0.1}$		$)SiO_3$	6	rhodonite + tr. bustamite
#13	$(Mn_{0.8}$	$Mg_{0.2}$		$)SiO_3$	4	rhodonite +pyroxmangite
#1	$(Mn_{0.75}$	$Mg_{0.25}$		$)SiO_3$	14	pyroxmangite + tr. quartz
#10	$(Mn_{0.75}$	$Mg_{0.225}$	$Ca_{0.025}$	$)SiO_3$	7	rhodonite
#2	$(Mn_{0.75}$	$Mg_{0.2}$	$Ca_{0.05}$	$)SiO_3$	14	rhodonite
#3	$(Mn_{0.75}$	$Mg_{0.15}$	$Ca_{0.1}$	$)SiO_3$	14	rhodonite + bustamite + tr. quartz
#4	$(Mn_{0.75}$	$Mg_{0.1}$	$Ca_{0.15}$	$)SiO_3$	14	rhodonite + bustamite
#5	$(Mn_{0.75}$	$Mg_{0.05}$	$Ca_{0.2}$	$)SiO_3$	49	bustamite + tr. rhodonite + tr. quartz
#6	$(Mn_{0.75}$	$Ca_{0.25}$		$)SiO_3$	46	bustamite
#14	$(Mn_{0.7}$	$Mg_{0.3.}$		$)SiO_3$	8	pyroxmangite
#12	$(Mn_{0.66}$	$Mg_{0.3}$	$Ca_{0.04}$	$)SiO_3$	3	rhodonite
#11	$(Mn_{0.66}$	$Mg_{0.26}$	$Ca_{0.08}$	$)SiO_3$	2	rhodonite + tr. bustamite
#15	$(Mn_{0.61}$	$Mg_{0.35}$	$Ca_{0.04}$	$)SiO_3$	4	rhodonite + pyroxmangite
#21	$(Mn_{0.6}$	$Mg_{0.25}$	$Ca_{0.15}$	$)SiO_3$	5	rhodonite + bustamite
#19	$(Mn_{0.6}$	$Mg_{0.2}$	$Ca_{0.2}$	$)SiO_3$	5	bustamite + tr. quartz
#20	$(Mn_{0.6}$	$Mg_{0.1}$	$Ca_{0.3}$	$)SiO_3$	4	bustamite
#16	$(Mn_{0.56}$	$Mg_{0.4}$	$Ca_{0.04}$	$)SiO_3$	6	pyroxmangite + rhodonite
#17	$(Mn_{0.51}$	$Mg_{0.45}$	$Ca_{0.04}$	$)SiO_3$	6	pyroxmangite
#18	$(Mn_{0.46}$	$Mg_{0.5}$	$Ca_{0.04}$	$)SiO_3$	5	pyroxmangite + kanoite
#22	$(Mn_{0.4}$	$Mg_{0.4}$	$Ca_{0.2}$	$)SiO_3$	3	kanoite + bustamite
#23	$(Mn_{0.4}$	$Mg_{0.3}$	$Ca_{0.3}$	$)SiO_3$	3	bustamite + kanoite
#24	$(Mn_{0.4}$	$Mg_{0.2}$	$Ca_{0.4}$	$)SiO_3$	5	bustamite + tr. kanoite
#25	$(Mn_{0.36}$	$Mg_{0.6}$	$Ca_{0.04}$	$)SiO_3$	3	kanoite
#40	$(Mn_{0.4}$	$Mg_{0.6}$		$)SiO_3$	5	kanoite

tr. : trace.

(Table 6)

1200°C 1 atm

#7	$MnSiO_3$				14	rhodonite
#9	$(Mn_{0.9}$	$Ca_{0.1}$	$)SiO_3$		14	rhodonite + bustamite
#2	$(Mn_{0.75}$	$Mg_{0.2}$	$Ca_{0.05}$	$)SiO_3$	10	rhodonite + tr. bustamite
#3	$(Mn_{0.75}$	$Mg_{0.15}$	$Ca_{0.1}$	$)SiO_3$	10	rhodonite + tr. bustamite
#12	$(Mn_{0.66}$	$Mg_{0.3}$	$Ca_{0.04}$	$)SiO_3$	10	rhodonite + tr. quartz
#21	$(Mn_{0.6}$	$Mg_{0.25}$	$Ca_{0.15}$	$)SiO_3$	10	bustamite + rhodonite
#16	$(Mn_{0.56}$	$Mg_{0.4}$	$Ca_{0.04}$	$)SiO_3$	10	rhodonite
#B	$(Mn_{0.5}$	$Mg_{0.5}$	$)SiO_3$		14	pyroxmangite
#40	$(Mn_{0.4}$	$Mg_{0.6}$	$)SiO_3$		10	pyroxmangite + bustamite
#18	$(Mn_{0.46}$	$Mg_{0.5}$	$Ca_{0.04}$	$)SiO_3$	10	pyroxmangite + rhodonite + tr. quartz
#32	$(Mn_{0.4}$	$Mg_{0.5}$	$Ca_{0.1}$	$)SiO_3$	10	rhodonite + pyroxmangite + bustamite
#22	$(Mn_{0.4}$	$Mg_{0.4}$	$Ca_{0.2}$	$)SiO_3$	10	bustamite + rhodonite
#23	$(Mn_{0.4}$	$Mg_{0.3}$	$Ca_{0.3}$	$)SiO_3$	10	bustamite
#24	$(Mn_{0.4}$	$Mg_{0.2}$	$Ca_{0.4}$	$)SiO_3$	10	bustamite
#25	$(Mn_{0.36}$	$Mg_{0.6}$	$Ca_{0.04}$	$)SiO_3$	10	pyroxmangite + tr. quartz

tr. : trace.

(Table 6)

800°C 4 kb

#102	$(Mn_{0.9}$ | $Ca_{0.1}$ | $)SiO_3$	8	rhodonite + tr pyroxmangite
#104	$(Mn_{0.85}$ | $Mg_{0.15}$ | $)SiO_3$	12	rhodonite
#106	$(Mn_{0.75}$ | $Mg_{0.25}$ | $)SiO_3$	11	rhodonite + pyroxmangite
#107	$(Mn_{0.55}$ | $Mg_{0.45}$ | $)SiO_3$	16	pyroxmangite + kanoite

tr. : trace.

900°C 4 kb

#102	$(Mn_{0.9}$ | $Ca_{0.1}$ | $)SiO_3$	9	rhodonite
#109	$(Mn_{0.85}$ | $Ca_{0.15}$ | $)SiO_3$	8	rhodonite + bustamite
#110	$(Mn_{0.5}$ | $Mg_{0.3}$ | $)SiO_3$	13	pyroxmangite

tr. : trace.

1000°C 4 kb

#106	$(Mn_{0.75}$ | $Mg_{0.25}$ | $)SiO_3$	10	rhodonite + pyroxmangite
#109	$(Mn_{0.85}$ | $Ca_{0.15}$ | $)SiO_3$	13	rhodonite + bustamite
#110	$(Mn_{0.5}$ | $Mg_{0.3}$ | $)SiO_3$	13	pyroxmangite

tr. : trace.

700°C 7 kb

#104	$(Mn_{0.85}$ | $Mg_{0.15}$ | $)SiO_3$	13	rhodonite + pyroxmangite

tr. : trace.

(Table 6)

700°C 10 kb

#101	$(Mn_{0.75}\ Ca_{0.25})SiO_3$	36	rhodonite + bustamite
#104	$(Mn_{0.85}\ Mg_{0.15})SiO_3$	42	pyroxmangite
#107	$(Mn_{0.55}\ Mg_{0.45})SiO_3$	16	kanoite

tr. : trace.

900°C 10 kb

#101	$(Mn_{0.75}\ Ca_{0.25})SiO_3$	35	bustamite + tr. rhodonite

tr. : trace.

1000°C 10 kb

#101	$(Mn_{0.75}\ Ca_{0.25})SiO_3$	35	bustamite

tr. : trace.

powder diffraction using a graphite monochromatized CuKα radiation. In the experiments using starting material of pyroxenoid mixture, the reaction direction was interpreted from the relative X-ray intensities of the reactant and product phases, since the phase changes were sluggish even at experimental temperatures.

Chemical compositions of run products were determined with an EDAX SW9100 electron microprobe in Hokkaido university. Standard samples were used for an quantitative analyses. The operating conditions were 15 keV accelerating voltage, 20 nA beam current, 200 second live time, and ZAF corrections were made for the quantitative analyses. Products were fixed on the glass plate with regine and polished with diamond paste. Because the run products are aggregates of the grains less than 5 μm in diameter, it was a little difficult to make point analyses on a single grain. At least 3 points analyses have been carried out on the same grain for accuracy.

2-3 Experimental results

In the Mn-rich portion of the system $MnSiO_3$-$MgSiO_3$-$CaSiO_3$, the following phase assemblages were observed depending on the compositions of starting materials and Pressure - temperature conditions : rhodonite solid solusion (rhd_{ss}), pyroxmangite solid solusion (pxm_{ss}), bustamite solid solusion (bus_{ss}), kanoite solid solusion (kan_{ss}), rhd_{ss} + pxm_{ss}, rhd_{ss} + bus_{ss}, bus_{ss}+kan_{ss}, rhd_{ss} + pxm_{ss} + bus_{ss} and pxm_{ss}+kan_{ss}. (Table 8).

The isothermal diagram at 700°C is shown in Fig. 9. The maximum amount of $CaSiO_3$ in $rhodonite_{ss}$ varies from 5 mol% to 10 mol%, and the upper limit of $MgSiO_3$ content decreased by 5 mol% with increasing pressure. The maximum amount of $CaSiO_3$ component dissolved in $pyroxmangite_{ss}$ decreases by 5 mol% and that of $MnSiO_3$ increases by 15 mol%. The miscibility gap between $rhodonite_{ss}$ and $pyroxemangite_{ss}$ shifts toward the $MnSiO_3$ side with increasing pressure. Thus the transition pressure of rhodonite to pyroxmangite increase with the decrease of $MgSiO_3$ component.

The isobaric diagram at 4kbar is shown in Fig. 10. With increasing temperature, the upper limit of $CaSiO_3$ content in $rhodonite_{ss}$ decreases by 5 mol% and $MgSiO_3$ content increase by 15 mol%. $Rhodonite_{ss}$ are spreads to the $MgSiO_3$ side. In $pyroxmangite_{ss}$, the $CaSiO_3$ content is independent of temperature and limited to within 5 mol%. Upper and lower limit of $MgSiO_3$ content in $pyroxmangite_{ss}$ increases by up to 10 mol% with increasing temperature. Thus the miscibility gap between $rhodonite_{ss}$ and $pyroxmangite_{ss}$ becomes narrow and shifts to the lower $CaSiO_3$ and higher $MgSiO_3$ side. $Bustamit_{ss}$ expands to the $MgSiO_3$ side

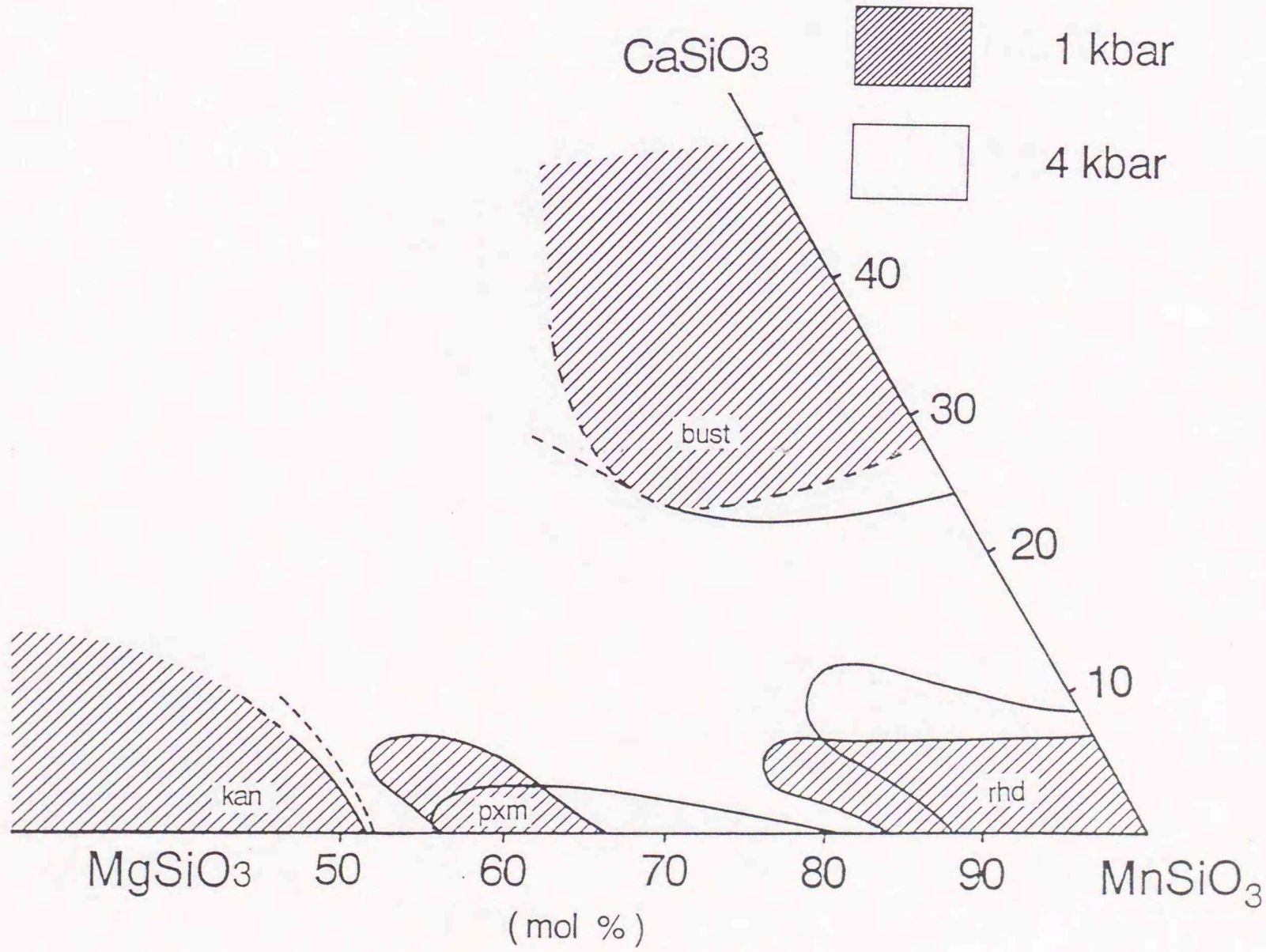

Fig. 9. Isothermal diagram at 700 °C. Hatched areas show the stability fields of rhodonite$_{ss}$, pyroxmangite$_{ss}$, bustamite$_{ss}$ and kanoite$_{ss}$ at 1 kb, and open areas show that at 4 kb.

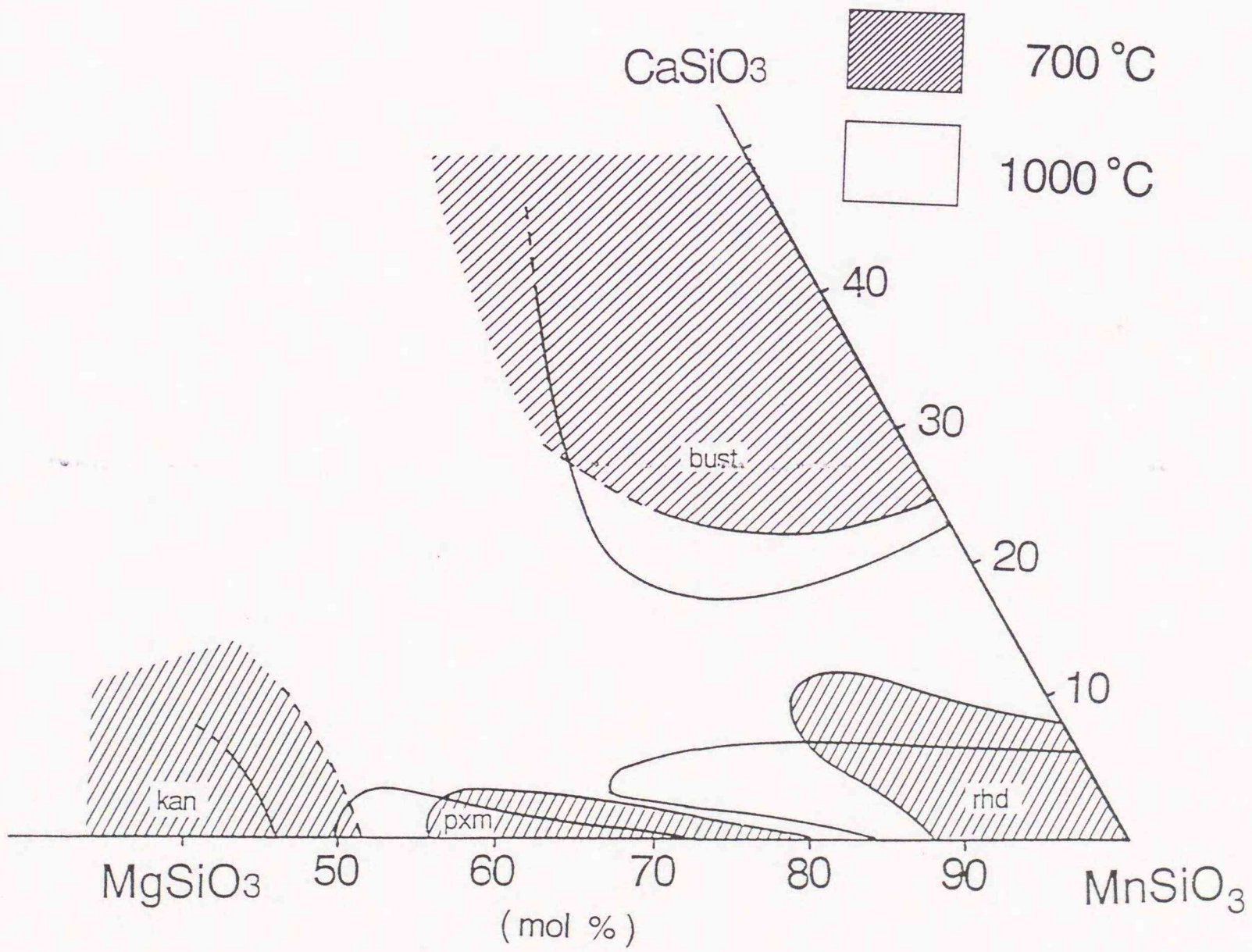

Fig. 10. Isobaric diagram at 4 kbar. Hatched areas show the stability fields of rhodonite$_{ss}$, pyroxmangite$_{ss}$, bustamite$_{ss}$ and kanoite$_{ss}$ at 700 ˚C, and open areas show that at 1000 ˚C.

and the miscibility gap between rhodonite$_{ss}$ and bustamite$_{ss}$ shifts by 15 mol% to the $MgSiO_3$ side. kanoite$_{ss}$ has a range of over 60 mol% $MgSiO_3$ content at 1000°C.

2-4 Discussion

A number of analyses of naturally coexisting pyroxmangite and rhodonite from Hokkaido, Japan are given in Fig. 11. To compare these analyses with the experimental results in the system $MnSiO_3$-$MgSiO_3$-$CaSiO_3$, natural samples whose $FeSiO_3$ content is lower than 5 mol% were chosen. The coexisting rhodonite and pyroxmangite pairs represent the mutual solubility limits of elements in the two phases. Some overlap may occur between pyroxmangite and rhodonite compositions in different localities, presumably due to the formation at different P-T conditions, since the present experimental studies reveal that the phase boundaries studied are sensitive to pressure and temperature. Comparison of natural data with experimental ones indicates that the compositional ranges of coexisting rhodonite and pyroxmangite from Tatehira mine show good agreement with the experimental results at 700°C-4kbar (Fig. 12). Kobayashi (1975) reported that the rocks of the Tatehira mine represent amphibole-granulite facies metamorphism, and this P-T condition is in agreement with the above experimental condition.

The compositional ranges of two phase regions from the Tokushibetu and especially, the Omatumae mine have less $MgSiO_3$ content, and they are nearly on the join $MnSiO_3$-$CaSiO_3$. Thus, pyroxmangite$_{ss}$ is close to the $MnSiO_3$ end member in the analyses of these mines. Maresch and Mottana (1976) showed that the phase transition between rhodonite and pyroxmangite in $MnSiO_3$ is represented by the equation : T(°C) = 378 + 20.2 P(kbar). Pyroxmangite is the higher pressure and lower temperature polymorph. We can estimate the pressure-temperature conditions of the formation of natural pairs of both phases with this equation. Assuming the formation temperature of these samples as 700°C, same as the Tatehira mine, the calculated formation pressure of these samples is as high as over

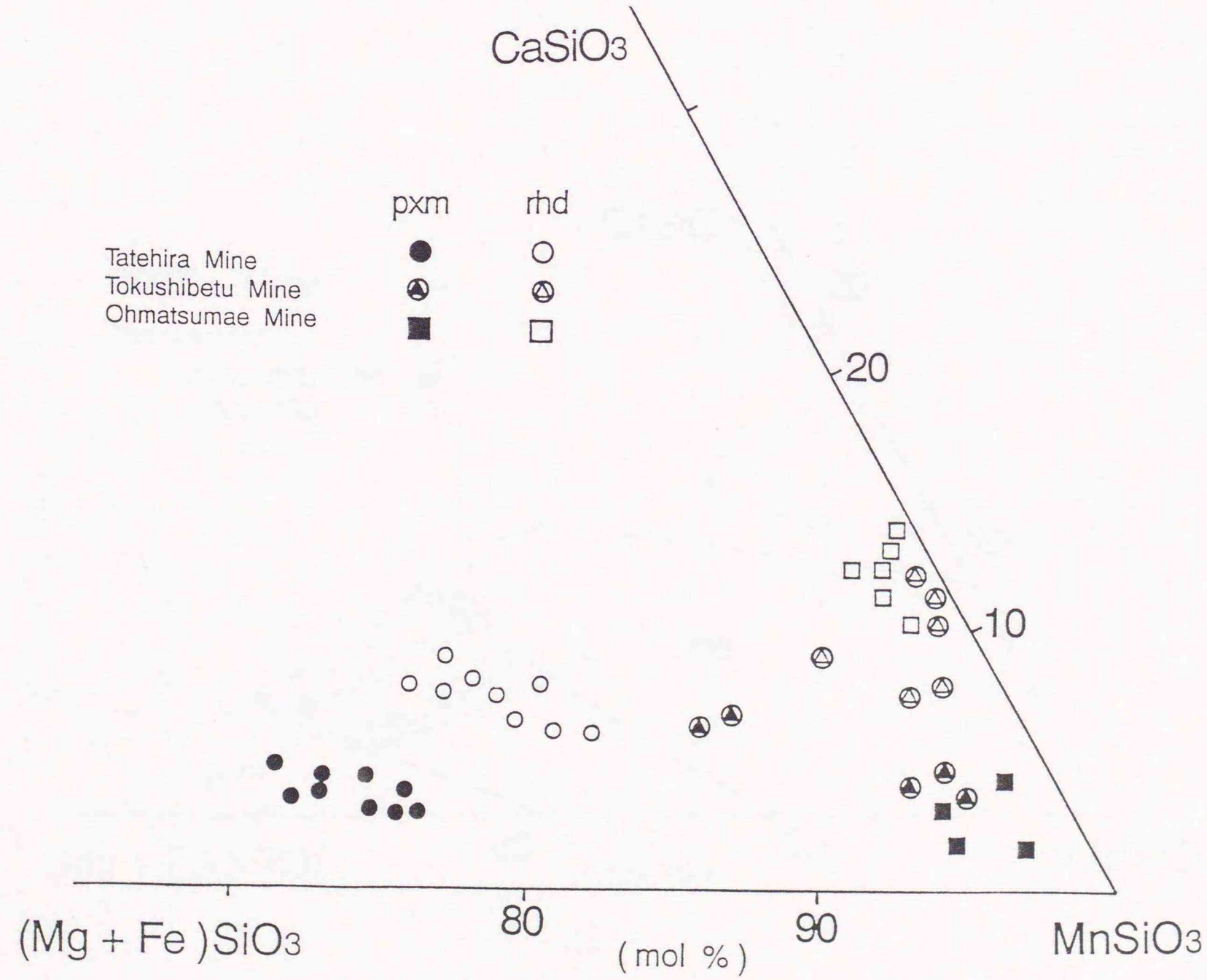

Fig. 11. $MnSiO_3$ - $CaSiO_3$ - $(Mg + Fe)SiO_3$ diagram shows compositions of coexisting natural rhodonite and pyroxmangite from Hokkaido, Japan. Filled and open symbol represents the compositions of pyroxmangite and rhodonite respectively.

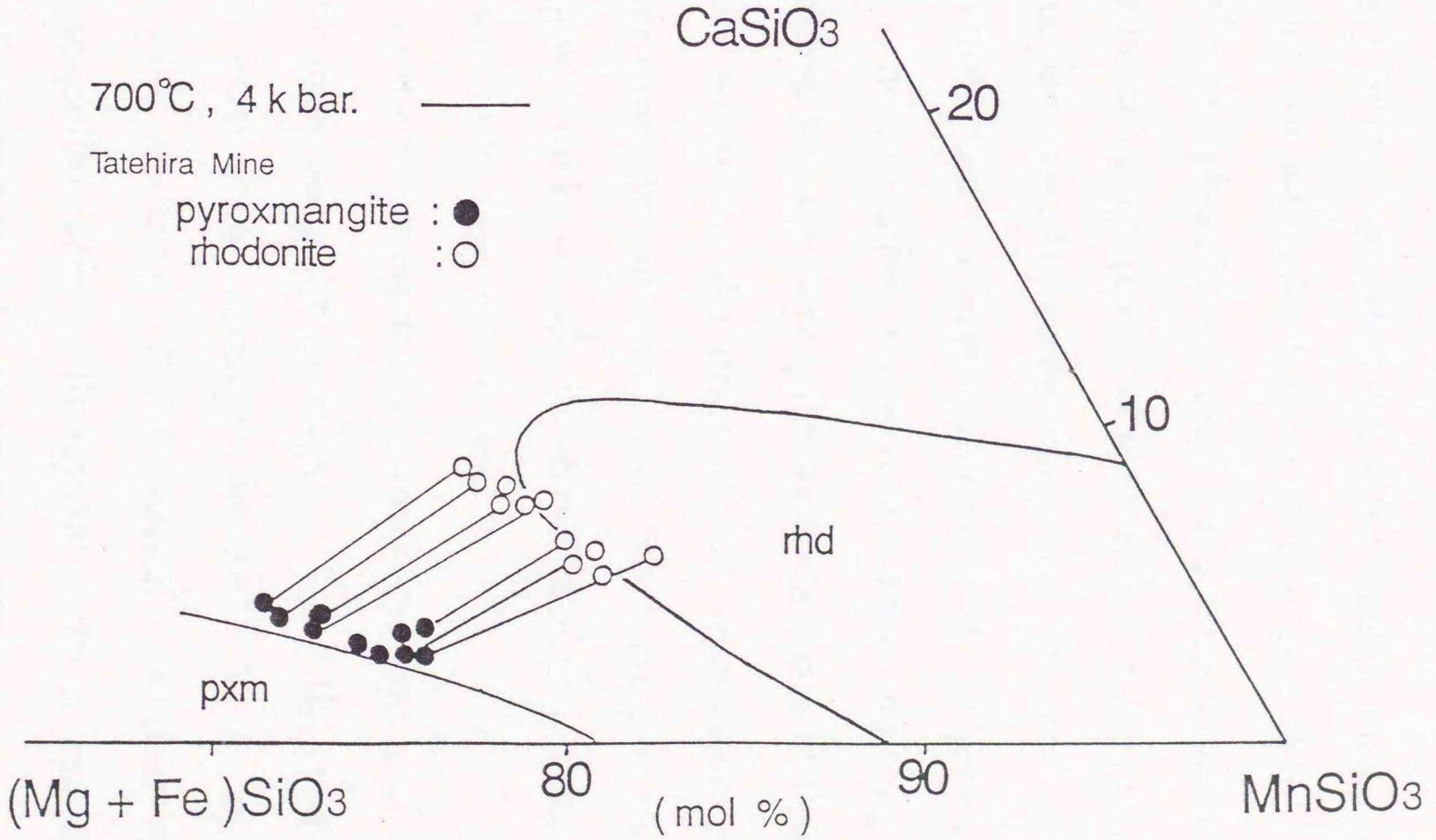

Fig. 12. Correlation of experimental results and natural sample from Tatehira mine. Filled and open circle represent compositions of natural pyroxmangite and rhodonite from Tatehira mine respectively. Coexisting pyroxmangite and rhodonite are joined by tie line. Stability fields of each minerals are the experimental results at 700 °C, 4 kb.

than 16 kbar. In the same manner as above, assuming the pressure as 4 kbar, the formation temperature becomes lower than 460 °C. It is not realistic that the pressure is much higher than 16kbar in the crustal metamorphic zone, it will be more reasonable to assume that the formation temperatures of the Tokushibetu and the Omatumae mine are lower than that of the Tatehira mine, 700 °C.

Because of the lack of the complete data about the compositions of coexisting pairs and phase boundaries, it has been impossible to determine the forming pressure and temperatures of pyroxenoids in the multicomponent systems from natural occurrences. The compositional deviations of the natural phases from the binary system, cause a large uncertainty of the pressure and temperature estimation if we adopt a simple binary model. By introducing the third component into the equation of KD, the author eliminated the above difficulty.

In the following, the pressure and temperature relations of natural rhodonite - pyroxmangite, and rhodonite - bustamite pair are estimated from the equation of K_D with the known X^j_{3rd} value. Still we can not obtain both temperature and pressure without further imformation.

Fig. 13 shows the result of the thermodynamic analyses of Tatehira mine and Bald Knob mine using the equation [A]. For the coexisting rhodonite and pyroxmangite pairs from Tatehira and Bald Knob mine, the formation temperatures were estimated. The formation condition of Tatehira mine is estimated as granulite facies (Kobayashi 1975), and the analyzed result corresponds to this pressure and temperature range.

Holdawey (1971) yields a pressure of Bald Knob mine as 5 kb. With this pressure estimation, the formation temperature of Bald Knob mine is estimated to be nearly 700 °C. Reasonable metamorphic temperatures may be calculated for the

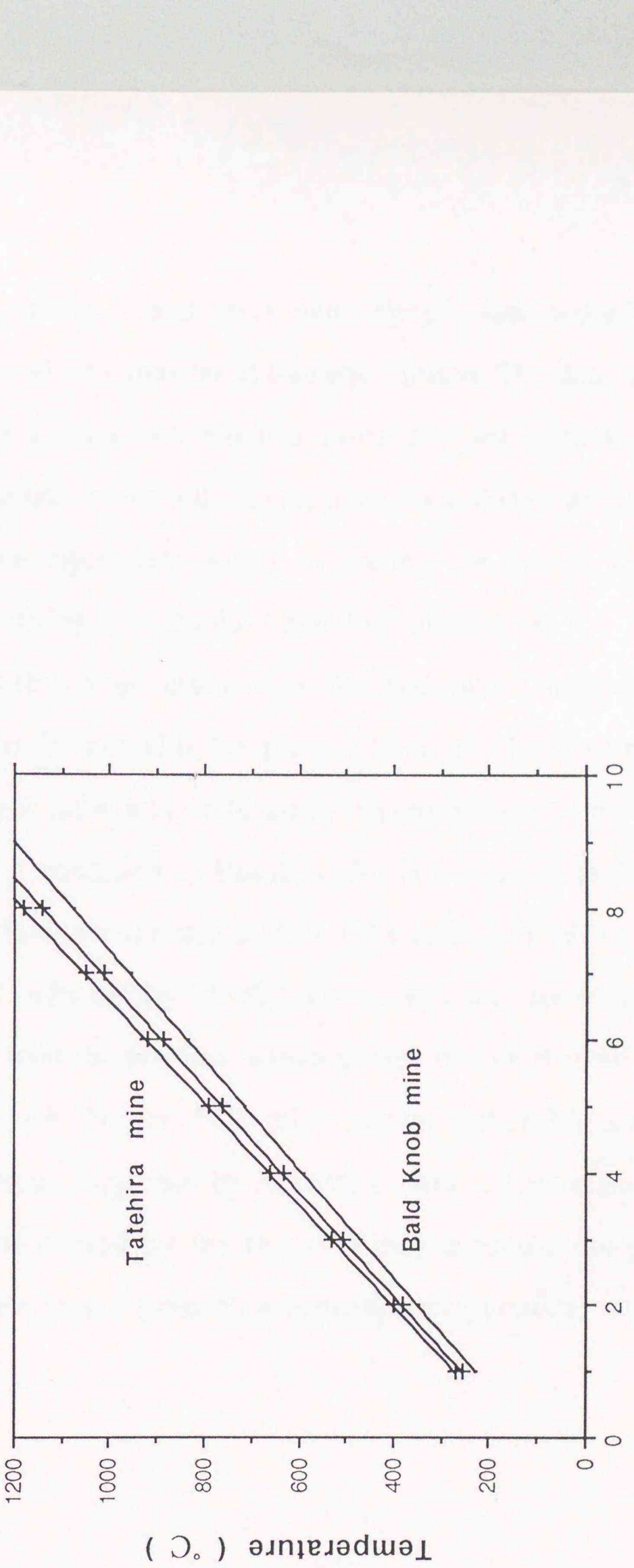

Fig. 13 Obtained pressure, temperature relations of rhodonite and pyroxemangite pairs of Tatehira mine and Bald knob mine.

occurrences of these mine. In both cases, pyroxmangite and rhodonite are present in subequal amounts and they may be in true equilibrium. The data of Ohmatsumae, Tokushibetsu, Buritirama and Koduru mine are not accurate enough with coexisting compositions to be applied to the analyses at this stage. These may reflect some chemical heterogeneities within or among the grains, a problem often encountered in coexisting pyroxenoids (Schults-Guttler, 1986).

Figure 14 shows the results of the thermodynamic analyses of rhodonite - bustamite pairs from Broken Hill, Ravinera di Sotto and Hoskins mine. The result from Andhra Pradesh mine was excluded the figure because of the same reason as above. The forming condition of Braoken Hill is estimated as 500 - 550 ˚C by Abrecht (1980), Ravinera di Sotto, as 620 ˚C by Abrecht (1979) and Hoskins as 450 - 500 ˚C, $P < 2$ kb by Ashley (1989). The present analyses of these mines show a good agreement with the previous works except that of Broken Hill mine. The result of analysis on Broken Hill mine shows rather higher pressure and temperature conditions suggested by Abrecht (1980). The mismatch of Broken Hill mine might be caused by the fact that they assumed the pressure of the formation as 2 kb and then estimated the formation temperature

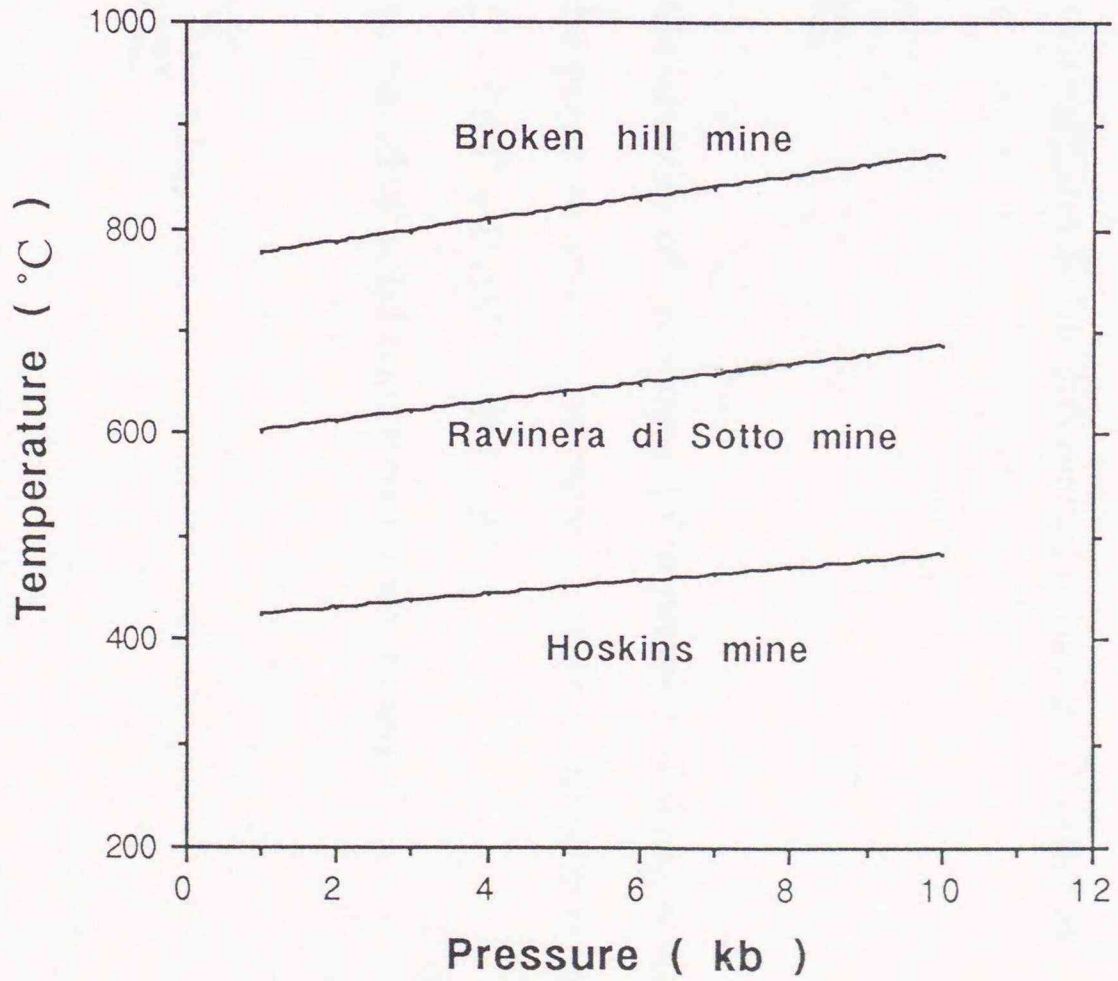

Fig. 14 Obtained pressure, temperature relations of rhodonite and bustamite pairs of Broken Hill mine, Ravinerra di Sotto mine and Hoskins mine.

2-5 thermodynamic analyses

Thermodynamics of element partitioning

In the Mn - Ca exchange reaction in the rhodonite - bustamite binary system,

Ca - rhodonite + Mn - bustamite $\leftrightarrow$ Mn - rhodonite + Ca - bustamite (1)

the equilibrium constant K for this reaction may be defined as

$$K = \frac{a_{Mn}^{rhd}}{a_{Ca}^{rhd}} \bullet \frac{a_{Ca}^{bust}}{a_{Mn}^{bust}} \qquad (2)$$

where a_j^i is the activity of component j in phase i. Taking a standard state of pure solids at the pressure and temperature of interest, then at equilibrium

$$\Delta G^{\circ}_{P,T} = \Delta U^{\circ} - T\Delta S^{\circ} + P\,\Delta V^{\circ} = -RT\,\ln K \qquad (3)$$

If the minerals are ideal solid solutions (a = x) then

$$K = \frac{X_{Mn}^{rhd}}{X_{Ca}^{rhd}} \bullet \frac{X_{Ca}^{bust}}{X_{Mn}^{bust}} = K_D \qquad (4)$$

where K_D is the distribution coefficient, X_{Mn}^{rhd} is the mole fraction of Mn in rhodonite and X_{Ca}^{bust} is the mole fraction of Ca in the bustamite etc. If the minerals are not idea, then $a = x\gamma$, where γ is defined as the activity coefficient. Thus

$$K = \frac{X_{Mn}^{rhd}}{X_{Ca}^{rhd}} \bullet \frac{X_{Ca}^{bust}}{X_{Mn}^{bust}} \bullet \frac{\gamma_{Mn}^{rhd}}{\gamma_{Ca}^{rhd}} \bullet \frac{\gamma_{Ca}^{bust}}{\gamma_{Mn}^{bust}} = K_D \bullet K\gamma \qquad (5)$$

The distribution coefficient (K_D) can be obtained from the mineral compositions, and in the case of ideal solid solutions, it can be considered a function of P, T only.

When the deviations from the ideal solid solution exist, however, this assumption is inadequate to explain the variations of the measured K_D with P, T changes, and the application of the more rigorous thermodynamic treatment to such equilibria requires a knowledge of the activity coefficients, γ, of the various solid solutions. There is as yet little data on γ for binary solid solutions of pyroxenoids.

In theory at least, it is possible to derive activity-composition relationships for different solid solutions from multicomponent experimental data by linear regression analysis of the non-ideal contributions in terms of regular solution model, Margules or interaction parameters (Thompson, 1967). Unfortunately, our knowledge of the mixing properties of binary solid solutions of prroxenoids is insufficient to justify such a rigorous treatment for reaction.

A limitation of our approaches is that the effect of nonideality in the rhodonite - pyroxmangite and rhodonite - bustamite solid solutions are cumulative in their effects on K_D. Thus, the approach adopted here is the derivation of a general equation as a practical geothermometer in terms of the variation in K_D with P, T, and X^j_{3rd}. This allocation of the third component effects on the binary system is justified for this approach as the variation in the third component contents of rhodonite with variations in P,T, and rock composition.

The variation of K_D with X^j_{3rd} and T as a geothermometer

Experimental data on the variation of K_D over a wide range of pressure, temperature and composition indicate that within the experimental error, K_D variation under any given P, T conditions can be satisfactorily accounted for by the associated change in X^j_{3rd} , where X^j_{3rd} is the mole fraction of the third component in phase j on the binary system. This variation in K_D can be quantified by assuming that at $X^j_{3rd} = 0$ the exchange reaction (6) may be considered ideal. Thus

$$\begin{aligned} \Delta G^0_{P,\,T}\,(X^j_{3rd} = 0) &= \Delta U^\circ - T\Delta S^\circ + P\,\Delta V^\circ \\ &= -\,RT \ln K \\ &= -\,RT \ln K_D \end{aligned} \qquad (6)$$

In this manner, all the third component effects on K_D at the given pressure can be accounted for by the following relationship

$$\ln K_D = a\, X^j_{3rd} + b \qquad (7)$$

The above constants (*a*) and (*b*) can be determined from the experimental data. Reliable data is available for the variation of K_D over a wide range of X^j_{3rd} .Data at 4 kb can be used for this relationship. A least squares fit to this data with the variation of temperature gives

$$\ln K_D = \frac{c}{T\,(K)} - d \qquad (8)$$

This equation can be conbined with that for the variation in ln K_D with X^j_{3rd} to derive the following equation,

$$\ln K_D = \frac{e\, X_{Ca}^{rhd} + f}{T\,(K)} - d \qquad (9)$$

The derivation of this equation assumes that ΔS^m (mixing entropy) is constant but ΔH^m (mixing enthalpy) is not 0 for the variation of X_{3rd}^j. In the thermodynamic sense, this is consistent with a symmetric regular solusion model of non - ideal substitution of the third component in the binary pyroxenoid system. This would be expected on the crystal chemical considerations as there is apparently no ordering of atoms in this substitution. The distribution of the divarent cation over all of the six coordinated these sites is considered to be random or nearly so.

The effect of pressure on K_D

Equation (9) is of limitted application without the knowledgement of the effect of pressure on K_D. There has been considerable discussion about the magnitude of this pressure effect, which may be related to the volume change of the exchange reaction (1).

$$\frac{\partial \ln k}{\partial P} = - \frac{\Delta V^0}{RT} \qquad (10)$$

This value, when combined with the above relationships, enables the derivation of the general equation to express the variation of K_D with P, T, and X_{3rd}^j.

$$\ln K_D = \frac{g\ X^{j}_{3rd} + h\ P\ (kb) + i}{T\ (K)} - d \qquad (11)$$

2-5-1 Pressure and temperature determination of coexisting rhodonite and pyroxmangite solid solutions

Temperature effect on K_D

The distribution coefficients of rhodonite - pyroxmangite equilibrium assemblages at different temperatures were calcurated from the experimental results. The equilibrium is taken as an exchange reaction of the form,

Mg - rhodonite + Mn - pyroxmangite

$\leftrightarrow$ Mn - rhodonite + Mg - pyroxmangite

for which the K_D is defined by

$$K_D = \frac{X^{pxm}_{Mg}\ (1 - X^{rhd}_{Mg})}{(1 - X^{pxm}_{Mg})\ X^{rhd}_{Mg}}$$

where

$$X_{Mg} = \frac{Mg}{Mg + Mn}$$

As is shown in Figure 15 , the 1 / T (T = obtained temperature, 973 - 1273 K) - $\ln K_D$ relation at 4 kb is approximately linear, and is defined by the equation

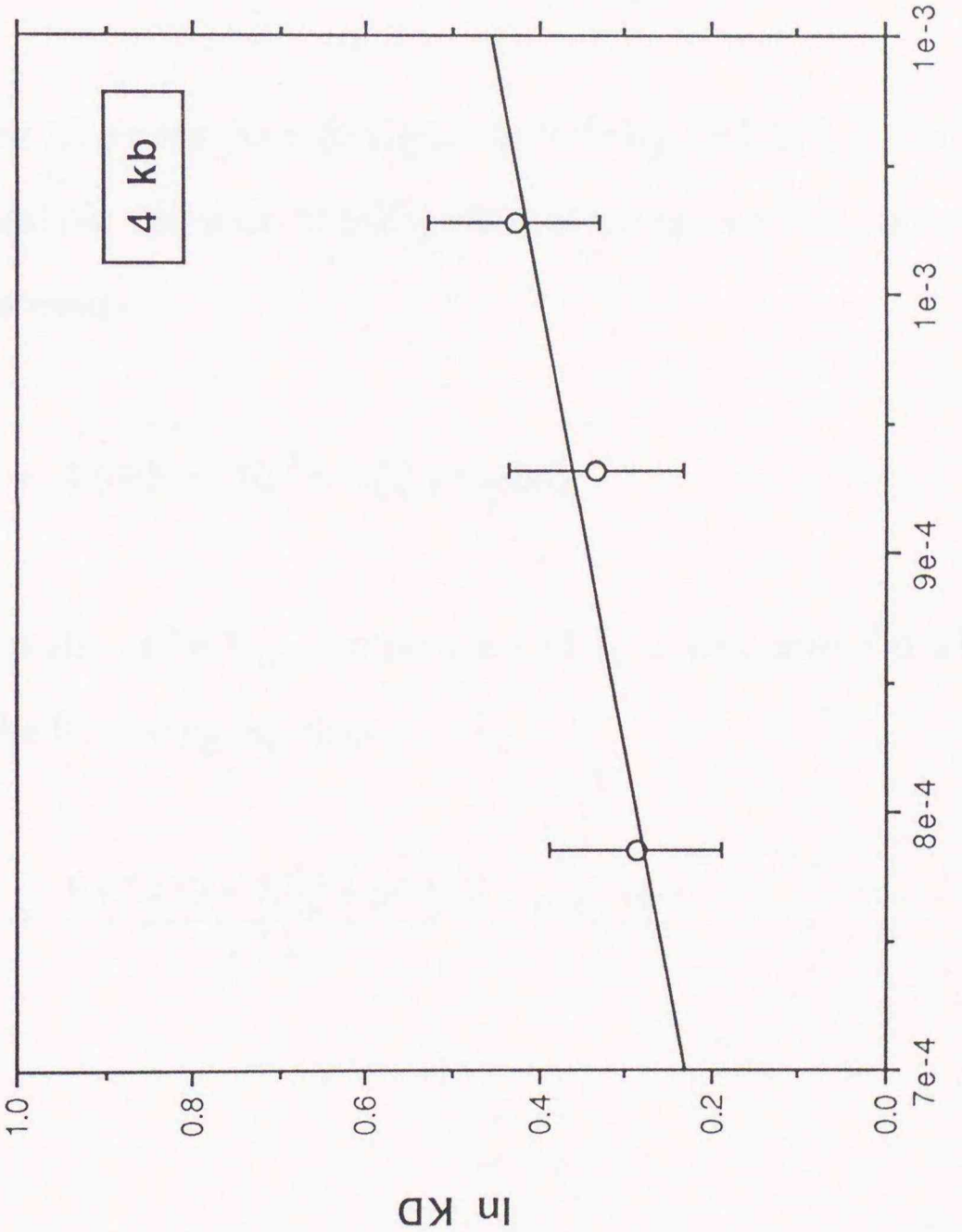

Fig. 15 $\ln K_D$ - 1/T plot of the 4 kb, $X_{Ca}^{rhd} = 0$ experimental data for the temperature range 700 - 1000 °C of rhodonite and pyroxmangite pair.

$$\ln K_D = \frac{560.87}{T\,(K)} - 0.1633 . \qquad [1]$$

Because the data sellected from Mn - Mg binary system, the equation [1] includes no effect of the third components, X_{Ca}^{rhd}.

X_{Ca}^{rhd} effect on K_D in MnSiO3 - MgSiO3 system

Figure 16 shows the relation between $\ln K_D$ and X_{Ca}^{rhd} at 700°C, 4 kb. There is a considarable variation of $\ln K_D$ value at the same condition with the different third components.

$$\ln K_D = 8.5829 \bullet 10^{-2} \bullet X_{Ca}^{rhd} + 0.4063 \qquad [2]$$

the equation of $\ln K_D$ - temperature [1] can be combined with this equation to derive the following equation,

$$\ln K_D = \frac{83.5459 \bullet X_{Ca}^{rhd} + 560.87}{T\,(K)} - 0.1633 \qquad [3]$$

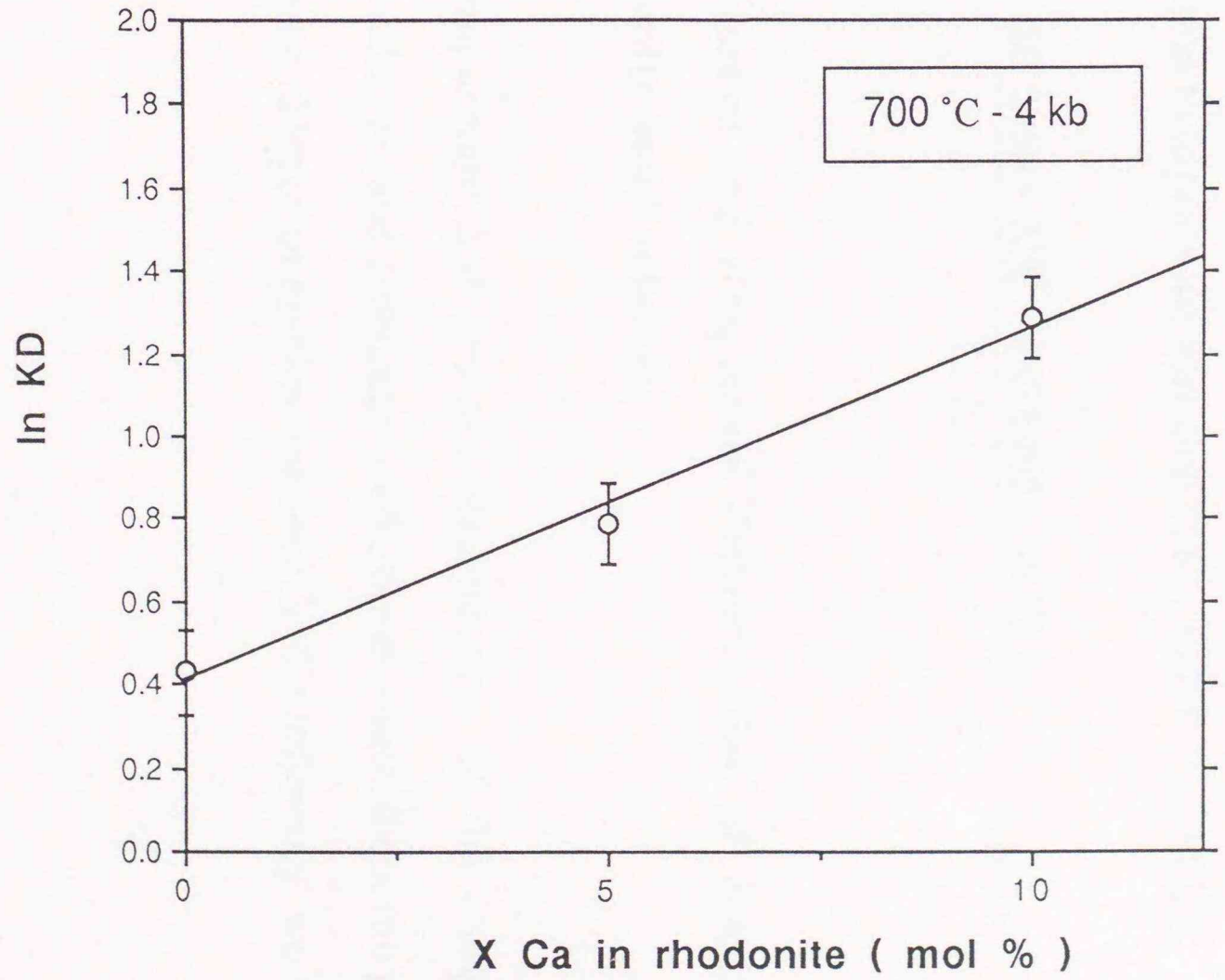

Fig. 16 Experimentally determined variation in $\ln K_D$ with X_{Ca}^{rhd} at 700 °C, 4 kb of rhodonite and pyroxmangite pair.

Pressure dependence of K_D

Figure 17 shows the pressure dependence of K_D. Least squares fit to the data becomes,

$$\ln K_D = -8.0909 \bullet 10^{-2} \bullet P\,(kb) + 0.7650 \qquad [4]$$

Equation [4] can be combinrd to equation [3]. Then, we can derive a general equation to express the variation of K_D with P, T, and X_{Ca}^{rhd}.

$$\ln K_D = \frac{83.5459 \bullet X_{Ca}^{rhd} + 245.8468 + 78.7558 \bullet P}{T\,(K)} - 0.1633$$

2-5-2 Pressure and temperture determination of coexisting rhodonite and bustamite solid solutions

The temperature and pressure dependences of the compositions of coexisting rhodonites and bustamites evoke the question about the possibility of using such assemblages as geothermometer. In the following, we examine this possibility.

Temperature effect on K_D

The distribution coefficients of rhodonite - bustanite equilibrium assemblages at different temperatures were calcurated from the experimental.

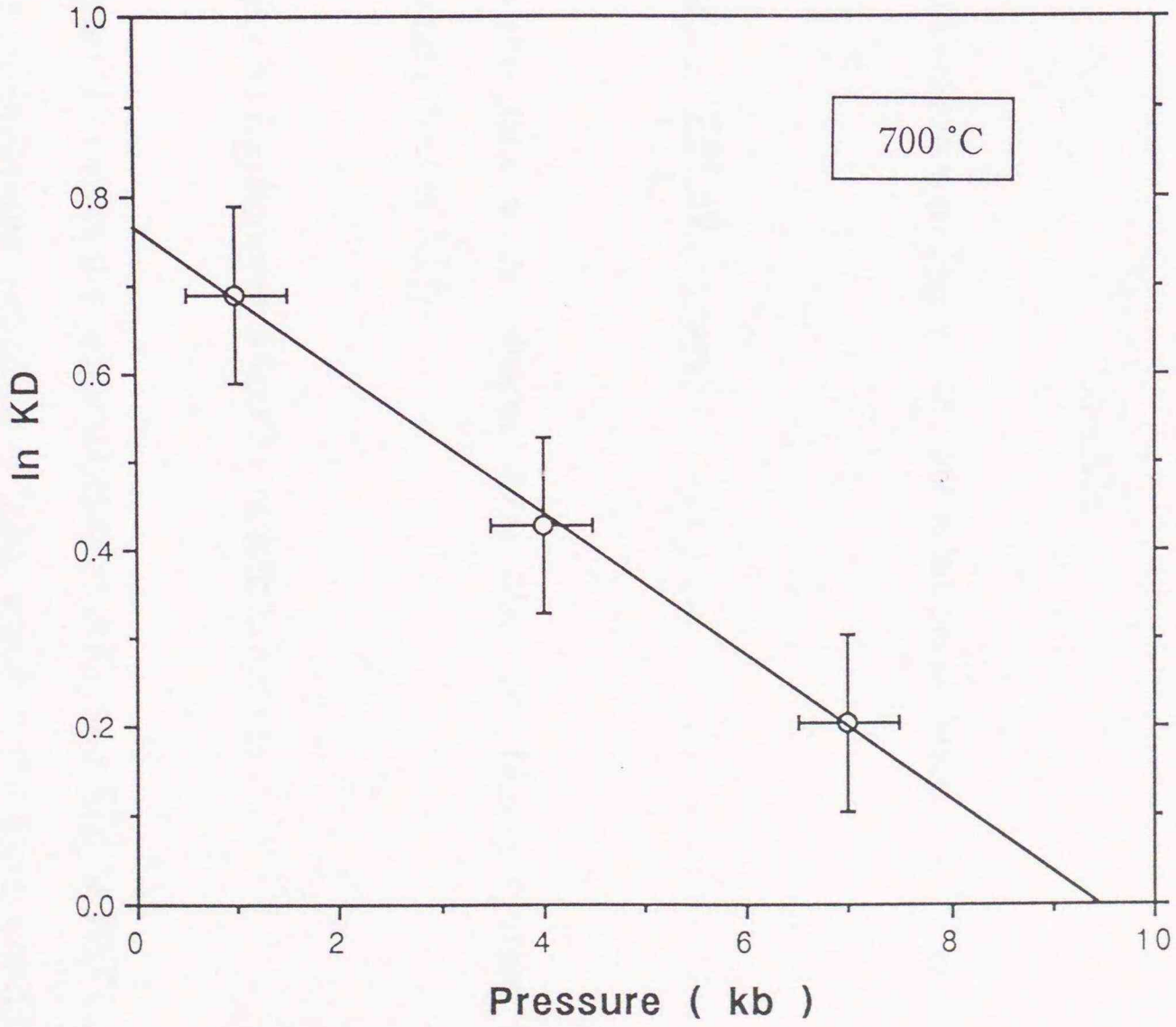

Fig. 17 Variation in experimentally determined $\ln K_D$ with pressure at 700 °C, $X_{Ca}^{rhd} = 0$ of rhodonite and pyroxmangite pair.

The equilibrium is taken from the following exchange reaction of the form

Ca - rhodonite + Mn - bustamite $\leftrightarrow$ Mn - rhodonite + Ca - bustamite

for which the K_D is defined by

$$K_D = \frac{X_{Ca}^{bust} (1 - X_{Ca}^{rhd})}{(1 - X_{Ca}^{bust}) X_{Ca}^{rhd}}$$

where

$$X_{Ca} = \frac{Ca}{Ca + Mn}$$

As is shown in Figure 18 ,the relation of $\ln K_D$ - 1 / T is defined by the equation,

$$\ln K_D = \frac{798.69}{T (K)} - 0.0802 . \qquad [1]$$

As the data were sellected from Mn - Mg binary system, the equation includes no effect of X_{Ca}^{rhd}.

X_{Mg}^{rhd} effect on K_D between MnSiO3 - CaSiO3 system

Figure 19 shows the relation between $\ln K_D$ and X_{Mg}^{rhd} at 700°C, 4 kb. There is also a considarable variation of $\ln K_D$ value at the same condition with the variation of the third component.

$$\ln K_D = 9.0260 \cdot 10^{-3} \cdot X_{Mg}^{rhd} + 0.7022 \qquad [2]$$

the equation [1] can be combined with this equation to derive the

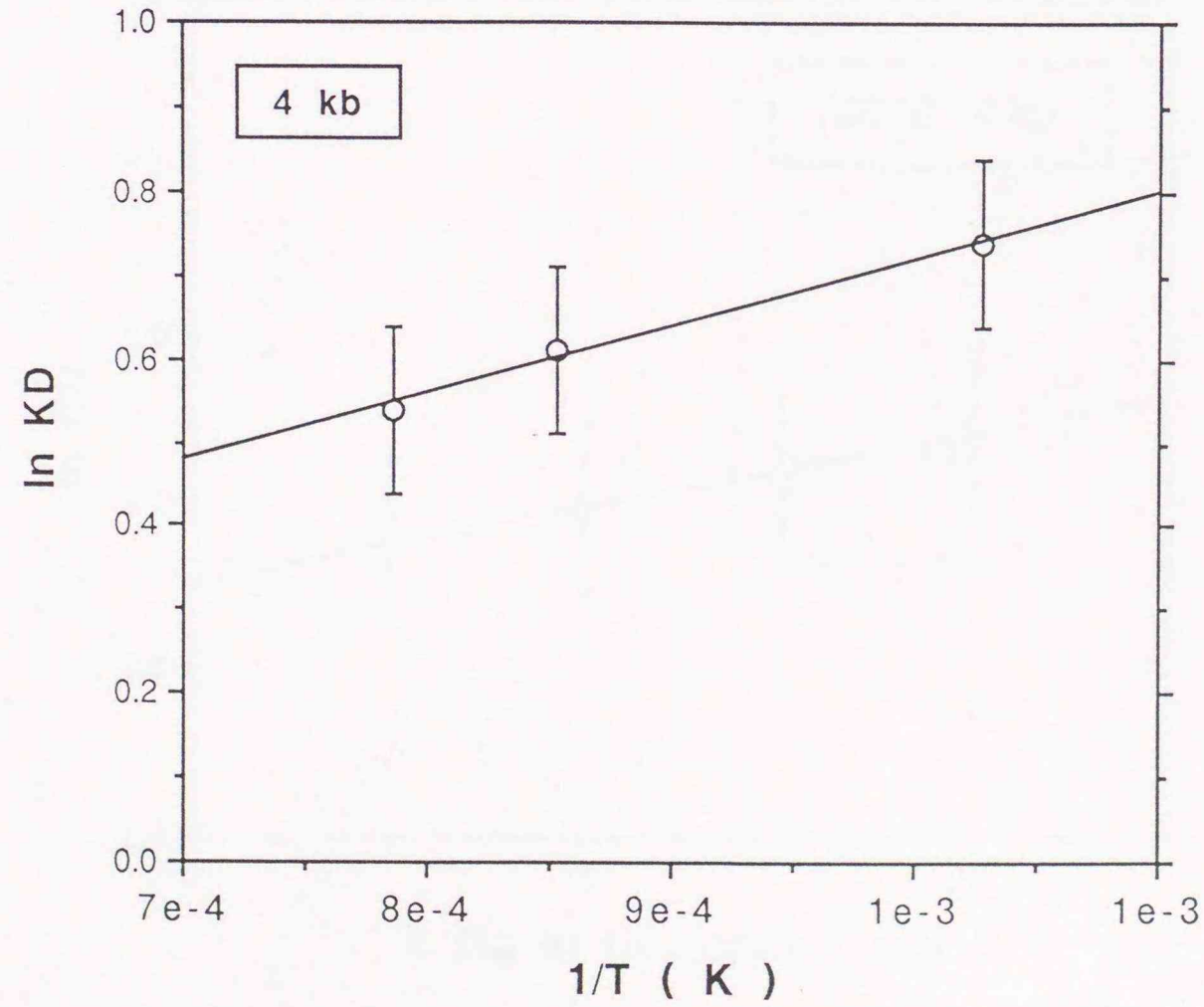

Fig. 18 $\ln K_D$ - 1/T plot of the 4 kb, $X_{Ca}^{rhd} = 0$ experimental data for the temperature range 700 - 1000 °C of rhodonite and bustamite pair.

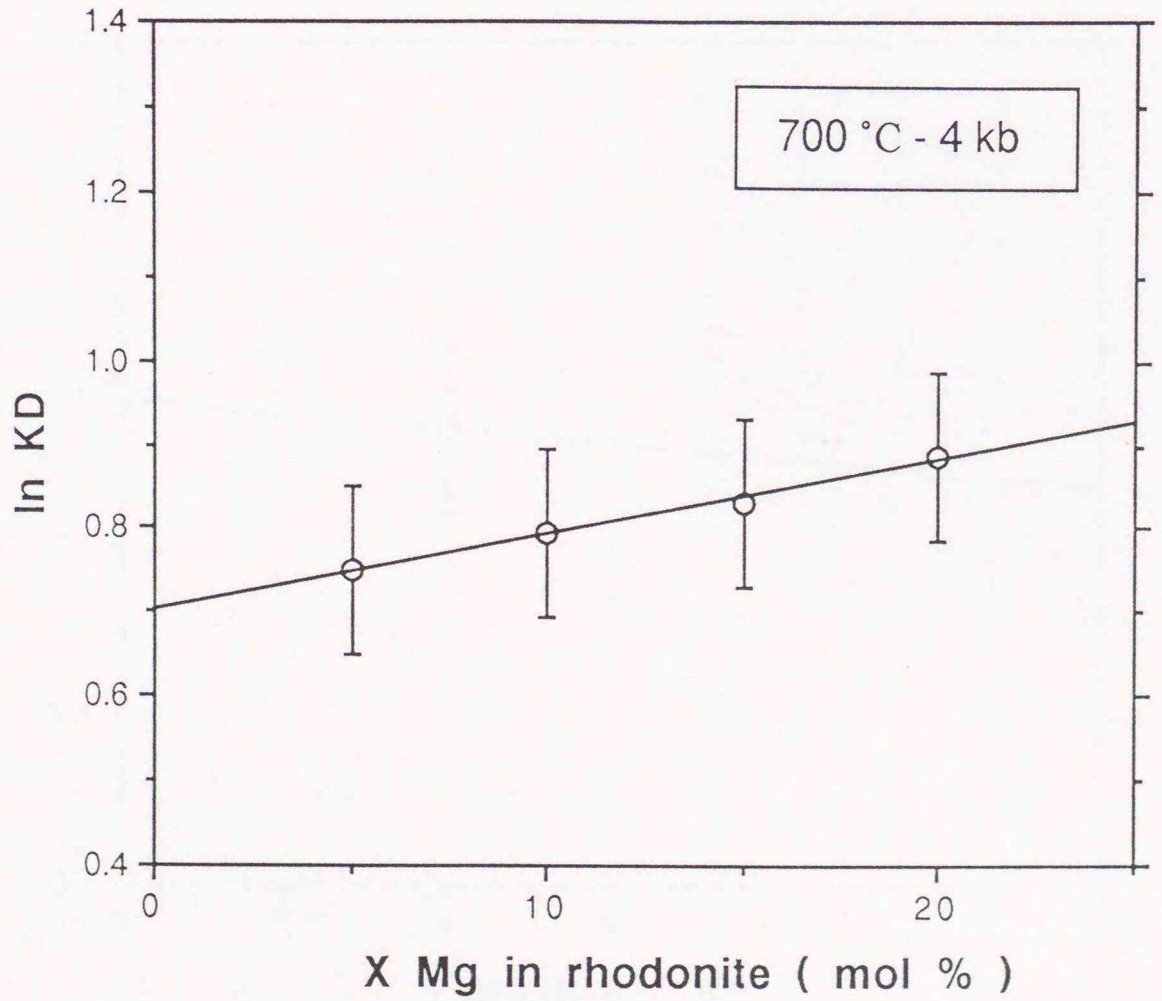

Fig. 19 Variation in experimentally determined $\ln K_D$ with pressure at 700 °C, $X_{Ca}^{rhd} = 0$ of rhodonite and bustamite pair.

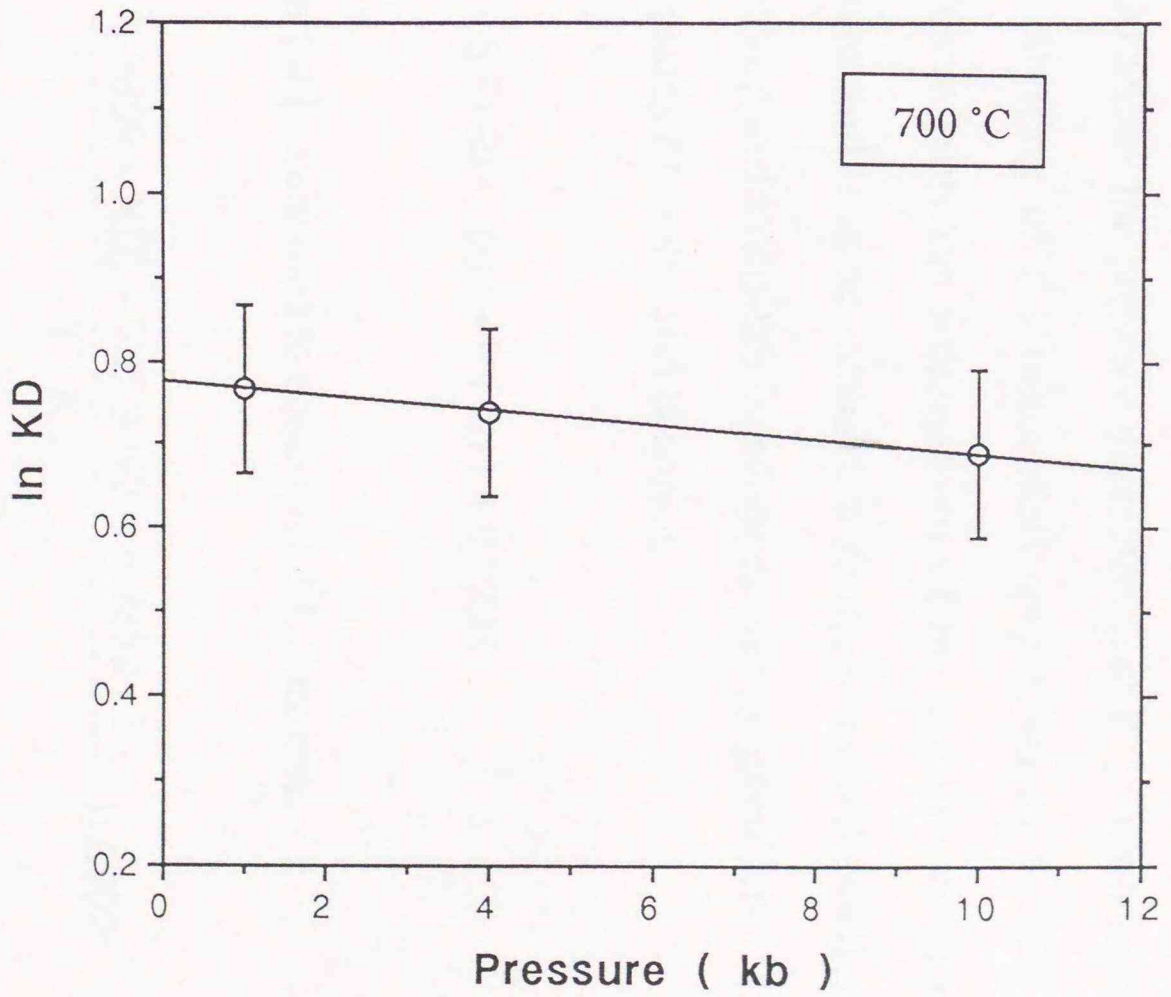

Fig. 20 Variation in experimentally determined $\ln K_D$ with pressure at 700 °C, $X_{Ca}^{rhd} = 0$ of rhodonite and bustamite pair.

following equation,

$$\ln K_D = \frac{8.7859 \bullet X_{Mg}^{rhd} + 798.69}{T\,(K)} - 0.0802 \qquad [3]$$

Pressure dependence of K_D

Figure 20 shows the pressure dependence of K_D. With increasing pressure a significant shifting of the miscibility gap towards the Ca-rich side was observed. This reflects the enlargement of the stability field of rhodonite at higher pressures and is in accordance with the observed smaller molar volume of rhodonite compared to bustamite of the same composition.

Least squares fit to the data becomes,

$$\ln K_D = -8.5166 \bullet 10^{-3} \bullet P\,(kb) + 0.7733 \qquad [4]$$

Equation [4], combined to equation [3], becomes

$$\ln K_D = \frac{8.7859 \bullet X_{Mg}^{rhd} + 765.5492 + 8.2852 \bullet P}{T\,(K)} - 0.0802$$

2-6 Conclusions

Stability fields for the rhodonite - pyroxmangite and rhodonite - bustamite pairs in the $MnSiO_3$-$MgSiO_3$-$CaSiO_3$ system were experimentally determined under the condition of 700 - 1200 ˚C and 0 - 10 kb.There was a significant change of the two phase regions depending on the pressure and temperature. From the microprobe analyses of the run products, the compositions of coexisting phases were comfirmed on the several P, T conditions. From these data, the distribution coefficient K_D was obtained as a function of temperature, pressure and the third component in addition to the binary system. It is essentially nessesary to use this function over the multicomponent system being these coexisting phases on. If the coexisting two phase (rhodonite - pyroxmangite, rhodonite - bustamite) were observed in natural occurrences, the resulted equation can be applied for the estimation of metamorphic conditions of manganese bearing rocks.

Summary

On the basis of the above results and discussions of the part 1 and part 2, present study is summarized as follows :

1 : Si - rich braunite from Hikari mine, southwestern Hokkaido, coexist with rhodochrosite and shows idiomorphic shape. The compositions of Si - rich braunite have zonal variations that represent the ideal braunite composition at the center of the crystal grain and the enrichment of the Si content at the rim.

2 : Experimental study carried out at 1100 °C in atmosphere to estimate the solid solubility of $MgSiO_3$ component to braunite show the solubility of the $MgSiO_3$ component as x = 0.2 in the formula of $(Mn^{3+}_{6-2x}Mg_xSi_x)\cdot Mn^{2+}SiO_{12}$. Over this solubility limit, Si - rich braunite coexist with tephroite which has the composition of $(Mn_{1.3}Mg_{0.7})SiO_4$.

3 : Braunite II from Wafangzi deposit, China shows a trend of the solid solution to neltnerite composition different from braunite composition.

4 : The mechanism of the substitution of silicon in the Si - rich braunite is considered to be the following ; the substitution of $2Mn^{3+} = Mg^{+2} + Si^{+4}$ occurs the A sheet not the B sheet, because the Ca content of natural samples from Hikari mine maintain the constant value regardless of the changes of other components.

5 : From the high - temperature, high - pressure experiments, two phase region of the rhodonite and pyroxmangite pair shifts toward the Mg - rich portion of the $MnSiO_3$-$MgSiO_3$-$CaSiO_3$ ternary system with the increase of pressure and/or the decrease of temperature. Meanwhile, two phase region of the rhodonite and bustamite pair shifts toward the Ca - rich side of this system with the increase of

pressure and/or the decrease of temperature.

6 : Using the experimental results, the author obtained the relations among pressure, temperature, X^{j}_{3rd} (third component) and K_D (distribution coefficient). This relationships can be applied to the pressure and temperature estimation of the formation of naturally coexisting rhodonite - pyroxemangite pairs or rhodonite - bustamite pairs.

7 : Estimated P, T conditions of several manganese deposits, usingthe above equations, show a good agreement with the previous works.

8 : It is expected that the presently unknown conditions of rhodonite - pyroxmangite pear or rhodonite - bustamite pairs can be solved using the results of this study.

Acknowledgements

The author gratefully acknowledges the help of Professor Kiyoshi. Fujino, Assistant Prof. Takeshi Kikuchi and Lecturer Hiroyuki Miura of Hokkaido University for their guidances and encouragement throughout the course of this study, as well as for careful review of the manuscript.

Many thanks are due to Professor Yu Hariya of Hokkaido Institute of Technology for valuable suggestions and discussions from early stage of this study. The author is also deeply grateful to Mr. Syoichi Terada who is technical officer of Hokkaido University, for his helpful advice and assistance in high pressure experiments. The author is very grateful to Mr. Nobuyoshi Miyajima and Mr. Shinichi Horikawa for help making the figures and also grateful to Mr. N. Tomioka and other students of Hokkaido University. This study could not have been accomplished without their supports.

Reference

Abs - Wurmbach I (1980) : Miscibility and compatibility of braunite $Mn^{2+}Mn^{3+}{}_6O_8SiO_4$, in the system Mn - Si - O at 1 atm in air. Contrib Mineral. Petrol., 71, 393 - 399

Abs - Wurmbach I, Peters Tj, Langer K, and Schreyer W (1983) : Phase relations in the system Mn - Si - O : an experimental and petrological study. Neues Jahrbuch Miner. Abh., 146, 258 - 279

Abrechit, J. and Peters, Tj. (1975) : Hydrothermal systhesis of pyroxenoids in the system $MnSiO_3$ - $CaSiO_3$ at Pf = 2 kb. Contrib. Miner. Petrol., 50, 241 - 246.

Abrecht J, Peters Tj, Sommerauer J (1979) Manganiferous mineral assemblages of Ravinella di Sotto, Valle Strona (Itary). Mem Scienze Geol, vol. XXXIII, 215-221

Abrechit, J. and Peters, Tj. (1980) : The miscibility gap between rhodonite and bustamite along the join $MnSiO_3$- $Ca_{0.6}Mn_{0.4}SiO_3$. Contrib. Miner. Petrol., 74, 261 - 276.

Akimoto, S. and Syono, Y. (1972) : High pressure transformations in $MnSiO_3$. Am. Min., 57, 76 - 84.

Ashley, P. M.(1989) : Geochemisty and mineralogy of tephroite-bearing rocks from the Hoskins manganese mine, New South Wales, Australia. Neues Jahrbuch Miner. Abh., 161, 1, 85-111

Banerjee, H., Miura, H. and Hariya, Y. (1988) : Stability of $RSiO_3$ phases in the manganese rich portion of the system MnO - MgO - FeO - SiO_2 - CO_2. Miner. J., 14, 93 - 94.

Baudracco-Gritti, C., Caye, R., Permingeat, F., and Protas,J.(1982) : La neltnerite $CaMn_6SiO_{12}$ une nowvelle espece minerale du groupe de la braunite. Bull. Mineral., 105, 161-165

Bhattacharyya, S.(1986) : Moneral chemistry and petrology of the manganese silicate rokes of Vizianagaram manganese belt, Andhra Pradesh. Journal Geological Society of India, 27, 169-184

Binns, RA(1968) : Asbestiform bustamite from a cavity lining within the Broken HIll lode, New South Wales. J. Geol. Soc. Aust 15, 1-8

Bohlen, S. R., Boettcher, A. L., Dollase, W. and Essene, E. J. (1980a) : The effect of manganese on olivine - quartz - orthopyroxene stability. Earth Planet. Sci. Lett., 47, 11 - 20.

Brown, P. E., Essene, E. J. and Peacor, D. R. (1980) : Phase relations inferred from field data for Mn pyroxene and pyroxenoids. Contrib. Miner. Petrol., 74, 471 - 425.

DE Villiers, J, E,. et al., (1967) : Distinction between two members of the braunite group. Am. Min., 65, 756 - 765

DE Villiers, PR, and Buseck, PB (1989) : Stacking variation and nonstoichiometry in the bixbyite - braunite polysomatic mineral group. Am. Min., 74, 1325 - 1336

Hariya, Y. and Kennedy, G. C. (1968) : Equilibrium study of anorthite under high pressure and high temperature. Amer. Journ. Sci., 266, 193 - 203.

Hino, H., Minato, T., and Kusakabe, Y. (1977) : Hydrothermal synthesis of braunite in the system MnOOH - SiO_2, Mn_3O_4 - SiO_2, and MnO_2 - SiO_2. Mineral. Fac. Eng. Kyoto Univ., 40, 16 - 29

Hodgson, C. J. (1975) : The geology and geological development of the broken hill lode, in the New Broken Hill Consolidated Mine Australia . Part II: mineralogy. Journal of the Geological Society of Australia, 22,Pt. 1,33-50

Holdway, M.J.(1971) : Stability of andulusite and the aluminum silicate phase diagram. Amer. Journ Sci., 271, 97-131.

Huebner, J. S. (1986) : Nature of phases synthesized along the join (Mg, Mn)$_2Si_2O_6$. Am. Min., 71, 111 - 122.

Ito, J. (1972) : Rhodonite - pyroxmangite peritectic along the join $MnSiO_3$ - $MgSiO_3$ in air. Am. Min., 57, 865 - 876.

Iwabuchi, Y. and Hariya, Y. (1985) : Phase equilibria on the jin $MgSiO_3$ - $MnSiO_3$ at high pressure and temperature. Miner. J., 12, 319 - 331.

Kakuda, Y., Uchida, E. and Imai, N. (1991) : Experimental studies on phase equilibria in the system $CaSiO_3$ - $MnSiO_3$ - (Ca, Mn)Cl_2 - H_2O by means of iron exchange. Mining Geology, 41, 339 - 349.

Kobayashi, H. (1975) : The metamorphic rocks of Tatehira, south west Hokkaido, Japan (I). (in Japanese). Mem. Fac. Lit. & Sci., Shimane Univ., Nat. Sci., 8, 105 - 113.

Liebau, F.(1962) : Die Systematik der Silikate. Naturwissensch. 49, 481-491

Mason,B. (1973) : Manganese silicate minerals from Broken Hill, New South Wales. J.Geol.Soc.Aust., 20, Pt. 4,397-404

Maresch, W. V. and Mottana, A. (1976) : The pyroxmangite - Rhodonite transformation of $MnSiO_3$ composition. Contrib. Miner. Petrol., 55, 69 - 79.

Momoi, H. (1968) : Some manganese pyroxenoids. Jour. Miner. Soc. Japan, 8, Spec. Issue, 2, 1 - 6 (in Japanese).

Momoi, H. (1973) : Natural and synthesized pyroxenoids in the system $MgSiO_3$ - $MnSiO_3$. Sci. Rept., Dept. Geol. Kyusyu Univ., 11, 251 - 256. (in Japanese)

Momoi, H. (1974) : Hydrothermal crystallization of $MnSiO_3$ polymorphs. Miner. J., 7, 357 - 373.

Momoi H, Hirowatari F, and Fukuoka M (1982) : Natural and synthetic braunite. Min. Pet. (in Japanese) 3, 281 - 289

Moore, P. B.and Araki, T. (1976) : Braunite : its structure and relationship to bixbyite, and some inshight on the genealogy of fluorite derivative structures. Am. Min. 61, 1226 - 1240

Muan, A. (1959a) : Phase equilibria in the system manganese oxide SiO_2 in air. Am. Jour. Sci. 257, 297 - 315

Nishizawa, O. (1972) : An experimental study on the partition of magnesium and manganese between olivine and orthopyroxene. Phys. Earth. Planet. Interior 6 : 377 - 384

Ogino, A., Uchida, E., Kakuda, Y. and Imai, N. (1992) : Experimental study on the phase equilibria in the system $CaSiO_3$ - $FeSiO_3$ - $MnSiO_3$ - (Ca, Fe, Mn)Cl_2 - H_2O by means of iro exchange at 600°C and 1 kbar. Mining

Geology, 42, 119 - 129.

Peters, Tj, Valarelli, J. V., Coutinho, J. M. V.,Sommerauer,J. and von Raumer, J. (1977) : The manganese deposits of Buritirama (Para, Brazil).Schweiz. mineral. petrogr. Mitt., 57, 313-327

Petersen, E. U., Anovitz, L. M. and Essene, E. J. (1984) : Donpeacorite, (Mn, Mg)$MgSi_2O_6$, a new orthopyroxene and its proposed phase relations in the system $MnSiO_3$ - $MgSiO_3$ - $FeSiO_3$. Am. Min., 69, 472 - 480.

Reinecke, T., Tillnanns, E., and Bernhardt H-J (1991) : Abswurmbachite, $Cu^{2+}Mn^{3+}_6(O_8/SiO_4)$, a new mineral of the braunite group:natural occurence, synthesis, and crystal structure, Neues Jahrb.Miner. Abh. 163,117-143

Schults-Guttler, R.(1986) : Constraints on thermodynamic data for the system $MnSiO_3$. Contr. Mineral. Petrol.

Sivaprakash, C. (1980) : Mineralogy of manganese deposits of Koduru and Garbham, Andhra Pradesh, India. Economic Geology ,75, 1083-1104

Thompson, J. B., Jr. (1967) : Thermodynamic properties of simple solutions. In, P. H. Abelson, Ed., Researches in Geochemistry, vol. 2, John Wiley and Sons, New York, 340-361

Thompson JB(1978) : Biopyriboles and polysomatic series. Am. Min. ,63, 239-249

Veblen, D. R.(1991) : Polysomatism and polysomatic series: A review and applications. Am. Min., 76, 801-826

Whittaker, E. J. W. and Muntus, R. (1970) : Ionic radic for use in geochemistry. Geochim. Cosmochim. Acta, 34, 945-956

Winter, G.A., Esseme, E. J., Peacor D. R.(1981) : Carbonate and pyroxenoids from the manganese deposit near Bald Knob, North Carolina. Am. Min. 66, 278-289

Yui S, Aoki M (1986) : On - line data reduction with personal computer. Science Report Hirosaki Univ., 33, 36 - 43.

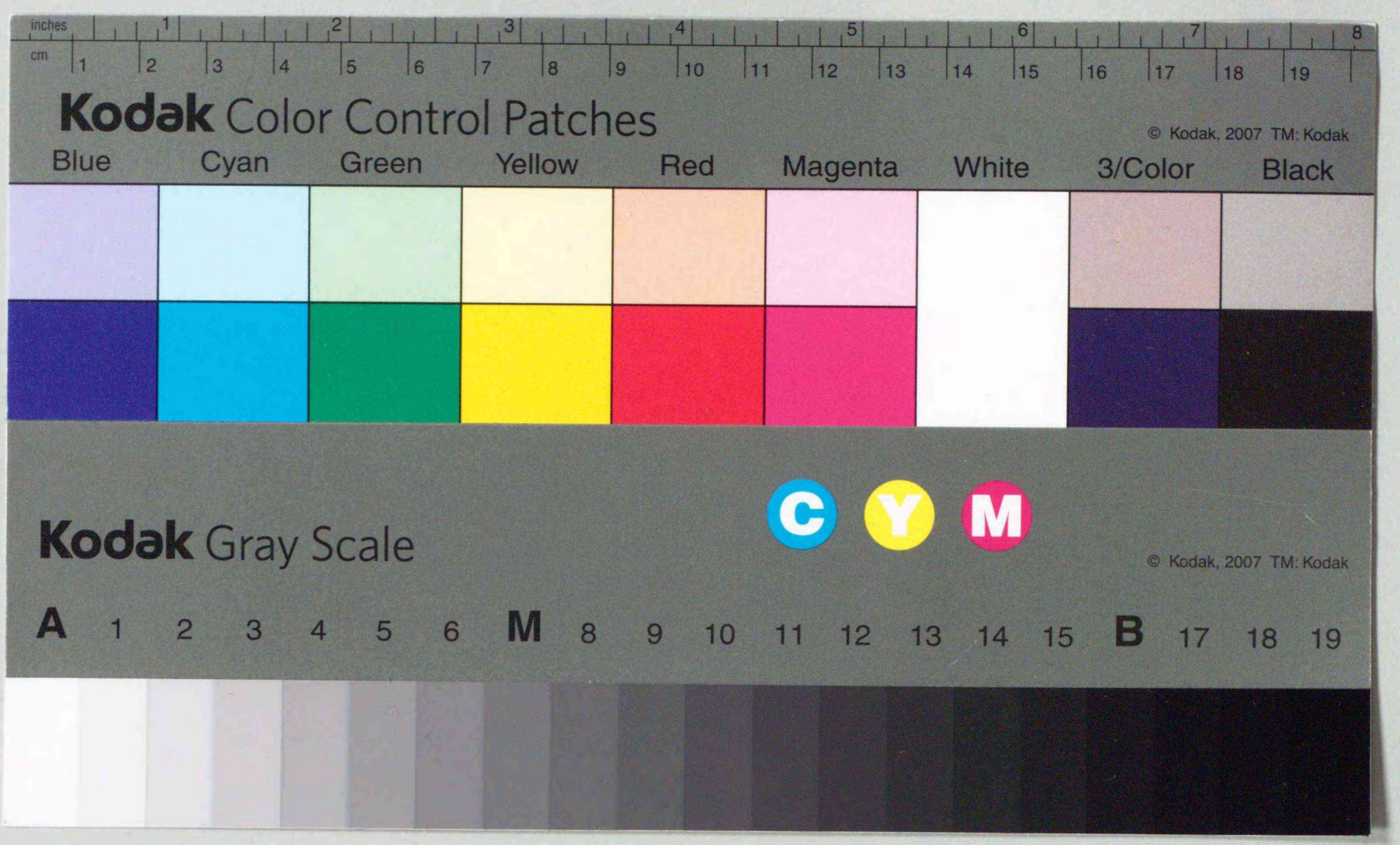
inches
cm
Kodak Color Control Patches
© Kodak, 2007 TM: Kodak
Blue
Cyan
Green
Yellow
Red
Magenta
White
3/Color
Black
Kodak Gray Scale
C
Y
M
© Kodak, 2007 TM: Kodak
A 1 2 3 4 5 6 M 8 9 10 11 12 13 14 15 B 17 18 19